

# Near-infrared absorption spectrum of the Ar–HD complex: Confrontation of theory with experiment

Felicja Mrugała

*Institute of Physics, N. Copernicus University, Grudziądzka 5, 87-100 Toruń, Poland*

Robert Moszynski

*Department of Chemistry, University of Warsaw, Pasteura 1, 02-093 Warsaw, Poland*

(Received 10 August 1998; accepted 16 September 1998)

Converged close-coupling calculations of the bound rovibrational levels, positions and widths of metastable states that predissociate rotationally, vibrationally, and via tunneling, transition intensities, and spectrum shape have been performed starting from accurate *ab initio* and empirical potential energy surfaces for Ar–HD. The computed transitions frequencies agree very well with the observed positions of lines in the recorded near-infrared spectra [A.R.W. McKellar, Faraday Discuss. Chem. Soc. **73**, 89 (1982); J. Chem. Phys. **105**, 2628 (1996)]. The agreement of the measured and calculated linewidths in the  $S_1(0)$  band is also good. Surprisingly, the *ab initio* potential reproduces the observed linewidths somewhat better than the empirical potential fitted to high-resolution infrared data of Ar–H<sub>2</sub> and Ar–D<sub>2</sub> [C. Bissonette *et al.*, J. Chem. Phys. **105**, 2639 (1996)]. As a result of the inclusion of some important transitions between the continuum states of the complex, a very good agreement with experiment is achieved for the shape of the  $S_1(0)$  band of the spectrum. Reliable theoretical predictions of the transition energies in the  $Q_1(1)$  band are also reported. © 1998 American Institute of Physics. [S0021-9606(98)01548-7]

## I. INTRODUCTION

Theoretical and experimental studies of van der Waals complexes provide important information about weak intermolecular forces between atoms and molecules. Weakly bound complexes of rare gas atoms with the hydrogen molecule are especially interesting, since they represent prototypes of systems governed by anisotropic interactions. In fact the Ar–H<sub>2</sub> molecule is probably the most thoroughly investigated van der Waals complex. Its first spectroscopic observation was reported by Kudian *et al.*<sup>1</sup> in 1965. Since then more and more refined measurements of the Ar–H<sub>2</sub> infrared spectra have been reported in the literature,<sup>2–9</sup> including experimental data for complexes of argon atoms with other isotopes of H<sub>2</sub>.

Measurements of high-resolution infrared spectra for Ar–H<sub>2</sub>, Ar–D<sub>2</sub>, and Ar–HD stimulated theoretical efforts<sup>10–14</sup> to determine an (anisotropic) potential energy surface for Ar–H<sub>2</sub> by directly fitting the observed infrared data and other quantities like hyperfine spectra,<sup>15</sup> state-to-state and total differential cross sections,<sup>16,17</sup> vibrational pressure shifting coefficients,<sup>18,19</sup> and second virial coefficients.<sup>20,21</sup> The potential energy surfaces obtained from direct fitting have been used to interpret various experimental data, in particular the mechanisms of the rotational<sup>22–32</sup> and vibrational<sup>33–36</sup> predissociation.

The most recent empirical potential energy surface for Ar–H<sub>2</sub>,<sup>14</sup> hereafter called the XC(fit) potential, was obtained by fitting to the infrared spectra of Ar–H<sub>2</sub> and Ar–D<sub>2</sub>,<sup>9</sup> as well as the temperature dependence of the second virial coefficients,<sup>20,21</sup> and collisional shift of the Raman lines of Ar–H<sub>2</sub>.<sup>18,19</sup> The fitting procedure adopted in Ref. 14 ensured that both the isotropic and anisotropic components were well

represented both in the region of the potential well and in the repulsive region. Additional calculations of the quantities not included in the fit (hyperfine spectra, and state-to-state and total scattering cross sections) were carried out. The level of agreement between the computed and measured values was impressive, and suggested that the empirical potential energy surface of Ar–H<sub>2</sub> (Ref. 14) is probably the most accurately determined of any atom–diatom potentials. Consequently, complexes of the argon atom with isotopes of H<sub>2</sub> constitute benchmark systems for *ab initio* calculations of the potential energy surfaces,<sup>37,38</sup> and for testing the accuracy of these surfaces in dynamical calculations.<sup>39</sup>

The *ab initio* potential energy surface of Ref. 37 has been computed using the symmetry-adapted perturbation theory (SAPT). See Ref. 40 for a recent review of the SAPT method and its applications. The accuracy of this three-dimensional potential (including the dependence on the vibrational coordinate of H<sub>2</sub>) was checked by comparison of the computed and measured line positions in the far and near-infrared spectra of Ar–H<sub>2</sub> and Ar–D<sub>2</sub>,<sup>39</sup> second virial coefficients,<sup>41</sup> state-to-state differential cross sections,<sup>14</sup> and vibrational pressure shifting coefficients.<sup>14</sup> The results of these calculations suggested that the well depth of the *ab initio* SAPT potential, its anisotropy around the van der Waals minimum, and its dependence on the vibrational coordinate of H<sub>2</sub> are essentially correct.

Various aspects of the Ar–HD spectroscopy were the subject of several experimental<sup>7,9</sup> and theoretical studies.<sup>26,28,42</sup> Among them, of particular interest is the rotational predissociation for the following reasons:

- (i) The predissociation widths have been measured for as many as 11 lines in the  $T$  and  $N$  branches of the  $S_1(0)$

band,<sup>7,9</sup> which is the largest set of data of this kind available for any of the hydrogen molecule–rare gas atom complexes.

- (ii) The predissociation widths are known to be sensitive probes of the anisotropy of the intermolecular potential in the repulsive wall region.<sup>13,24,43</sup> The most important first-order anisotropy arises from the asymmetric isotopic substitution, mostly from the isotropic and the leading anisotropic terms of the potential for Ar–H<sub>2</sub>. Although no systematic analysis of the relative importance of these terms in the predissociation dynamics of Ar–HD has been given thus far (cf. Ref. 26), there are good reasons to believe that the isotropic term, strictly its derivative,<sup>42</sup> is the decisive one. Therefore, the predissociation widths should be regarded as particularly sensitive probes of the shape of the isotropic part in the region of the repulsive wall. The correctness of this part, strictly speaking of its dependence on the diatomic vibrational coordinate, has been the most questioned feature of the previous (TT<sub>3</sub>) empirical model of the potential for Ar–H<sub>2</sub>.<sup>13,14</sup>
- (iii) In spite of the impressive progress which has been made in developments of efficient iterative procedures for the inversion of spectroscopic data into appropriate intermolecular potentials for van der Waals complexes (cf. Ref. 44), there are still difficulties in exploiting the experimental predissociation widths in these procedures. Because of that the newest empirical potential for Ar–H<sub>2</sub> could not be explicitly fitted to the measured widths of Ar–HD. Therefore, even this potential may not be sufficiently reliable to describe the rotational predissociation; at least, its adequacy in this respect has to be checked.

Another aspect of the Ar–HD dynamics of special interest for this work concerns quasi-bound states (orbiting resonances) and the effects of transitions from these states on the shape of the absorption spectrum. Such effects are certainly observed in the S<sub>1</sub>(0) band of the spectrum. However, no transition from initially quasi-bound state was accounted for in the theoretical simulation of the Ar–HD spectrum shape carried out by Kidd and Balint-Kurti,<sup>28</sup> the only one published thus far. Some consequences of this omission are easy to indicate: fewer lines appeared in the simulated spectrum. Less obvious is, however, how the relative intensity of the lines is altered, especially when transitions from broader states, more free- than bound-free in character, are included. Thus, a new simulation of the spectrum shape, which would account for all elements of the dynamics relevant for the absorption process, is desirable. Confrontation of the results of such a simulation with experiment seems to be a good opportunity for a comprehensive assessment of the present state of the theory. Not only the accuracy of the basic electronic structure ingredients, especially of the newest intermolecular potentials, can be verified in this way, but also the abilities of the close-coupling computational techniques of

nuclear dynamics (see Refs. 45,46 for recent reviews) to deal with phototransitions between multichannel continuum states can be severely tested.

Surprisingly, neither the empirical XC(fit) nor the *ab initio* SAPT potentials were tested in calculations of the positions, widths, and intensities of lines in the near-infrared spectrum of Ar–HD. In this paper we fill this gap, and report a detailed theoretical study of the near-infrared absorption spectrum of the Ar–HD complex and of the aforementioned aspects of the dynamics of this complex starting from the empirical XC(fit) and *ab initio* SAPT potentials. Whenever possible, the results of the study will be confronted with the experimental data.<sup>7,9</sup> Since the close-coupling approach applied in the calculations is believed to be nearly exact, any discrepancy between theory and experiment with respect to the positions and widths of the spectral lines will be attributed to some deficiencies of the intermolecular potentials. Thus, our results confronted with the experimental data will give an additional insight into the accuracy of the empirical and *ab initio* potentials. An outcome of our study will be also the first theoretical predictions of the line positions (and widths) in the Q<sub>1</sub>(1) band which may be of some use in future experimental work.<sup>47</sup> Finally, the shape of the Ar–HD spectrum in the S<sub>1</sub>(0) band, including the most important transitions between the continuum states of the complex, will be simulated. A comparison with both the previously simulated and observed shapes will be made and an assignment of the peaks discernible in the middle part of the observed band will be attempted.

The plan of this paper is as follows. Section II starts with a general characterization of the interaction-induced absorption in the Ar–HD gas mixtures which is based on the findings of the well-known experimental and theoretical research quoted above, and includes some new results of this work. Next, a brief description of the line shape theory in the interaction-induced absorption is given with the intent of summarizing and unifying the two important developments which provide the framework for the exact calculations of this work; the photodissociation theory of triatomic molecules of Balint-Kurti and Shapiro<sup>48,49</sup> and the rigorous treatment of the collision-induced spectra sketched in Refs. 50,51. The formula for the absorption line shape, derived from the (detailed) bound-to-free and free-to-free phototransition amplitudes for atom-diatom complexes, is presented in a concise form, appropriate for numerical evaluation with the help of the established invariant embedding methods of molecular scattering (cf. Ref. 46). Some useful formulas are also enclosed for determination of the positions and widths of the bound and metastable states with these methods. In Sec. III a short characterization is made of the dynamics of atom-diatom van der Waals complexes and specific aspects of the Ar–HD dynamics are discussed. In Sec. IV some technical details concerning the numerical calculations are given. Finally, in Sec. V the results of our calculations are presented, analyzed, and confronted with the available experimental data.<sup>7,9</sup>

## II. INTERACTION-INDUCED ABSORPTION OF THE Ar–HD GAS MIXTURE: AN OUTLINE OF THE LINE SHAPE THEORY

The (excess) absorption of light of frequency  $\omega$  caused by the interaction of the HD molecules with the Ar atoms in a low density gas mixture at a temperature  $T$  is characterized by the binary absorption coefficient,<sup>52</sup>  $\alpha(\omega, T) = n_{\text{HD}} n_{\text{Ar}} (1 - e^{-\hbar\omega/k_B T}) V \sigma(\omega, T)$ , which, apart from the respective number densities,  $n_{\text{HD}}$  and  $n_{\text{Ar}}$ , the factor  $(1 - e^{-\hbar\omega/k_B T})$  accounting for the stimulated emission, and the volume  $V$ , involves the photoabsorption cross section  $\sigma(\omega, T)$  for all the transitions undergoing in the Ar–HD complex from its thermally populated rovibro-translational states. These transitions are mediated by the collision-induced (component of the) electric dipole moment of the complex,  $\bar{\mathbf{d}}$ , in the way prescribed by the following golden rule based formula for  $\sigma$ :

$$\sigma(\omega, T) = \frac{4\pi^2\omega}{c} \sum_{i,f} P_i(T) |\langle f | \boldsymbol{\epsilon} \cdot \bar{\mathbf{d}} | i \rangle|^2 \delta(E_f - E_i - \hbar\omega). \quad (1)$$

Here  $\boldsymbol{\epsilon}$  denotes the direction of the electric vector of the incident light wave,  $|i\rangle$  and  $|f\rangle$  stand for the initial and final rovibro-translational states of the complex,  $E_i$  and  $E_f$  are the energies of these states, and  $P_i$  is the population of the initial state, i.e., the normalized Boltzmann factor.

The sum over the initial states includes all bound and continuum (free) states of the complex and the final state sum runs over all the states allowed by the energy conservation. For  $\omega$  in the near-infrared range, transitions of two kinds, free-free and bound-free, contribute to  $\sigma(\omega)$ , hereafter called the absorption spectrum ( $T$  is omitted as being fixed). The predominant free-free transitions determine the overall intensity of the spectrum, the most pronounced features of which are, as shown in Fig. 1 of Ref. 6, the broad lines centered around the frequencies of the  $Q(0)$ ,  $Q(1)$ ,  $S(0)$ , and  $S(1)$  transitions of the fundamental band of HD. The mean ‘‘time of spectroscopic interaction’’<sup>52</sup> within the Ar+HD collision complex, reflected by the widths of these lines ( $\approx 100 \text{ cm}^{-1}$  at  $T=87 \text{ K}$ ), is of the order of several  $10^{-14} \text{ s}$  and varies like  $T^{-1/2}$ . Continuum states characterized by the collision lifetimes<sup>53</sup> excessively larger than those quoted above are responsible, as participants of the bound-free and, to a lesser extent, of the free-free transitions, for the fine structures atop the broad lines of the spectrum, shown in the same figure and, with a better resolution in Figs. 7 and 8 of Ref. 7 and Fig. 11 of Ref. 9. These continuum states are associated with metastable states of the Ar–HD van der Waals molecules present in some (small) concentration in the gas. The metastable states involved can be divided into three groups differing in the leading mechanism of their decay; (i) the states predissociating via internal rotation-to-translation and (ii) internal vibration-to-translation energy transfer—the so-called Feshbach resonances, and (iii) the quasi-bound states decaying by tunneling through centrifugal barrier—shape (orbiting) resonances. The characteristic decay times for the rotational and vibrational predissociation in Ar–HD are  $\approx 5 \cdot 10^{-12}$  and  $\approx 5 \cdot 10^{-5} \text{ s}$ , respectively (the latter being the theoretical estimate of this work), and the

decay times of the (purely) tunneling states which are significant as initial states of the free-free transitions vary from  $10^{-4}$  down to  $10^{-12} \text{ s}$  (as it will also be shown in the present work). The decay times determine essentially the duration of the spectroscopic interactions causing absorption by van der Waals complexes. The observed widths of lines in the van der Waals part of the Ar–HD absorption spectrum<sup>7,9</sup> do reflect, however, only the shortest of these times, related to the rotational predissociation, and mostly in circumstances when a single transition can be assigned to a line. Such circumstances occur in the  $S_1(0)$  band of the spectrum. Actually, slightly faster rotational predissociation could be observed in the  $Q_1(1)$  band if it were not so heavily overlapped by the more intense  $Q_1(0)$  band (cf. Fig. 7 of Ref. 7). Slightly slower, in turn, rotational predissociation can be expected for the  $S_1(1)$  band. However, no sufficiently accurate picture of this band (cf. Ref. 6) has been published thus far to check this expectation. The widths due to the slow vibrational predissociation, which is the primary decay mechanism in the  $Q_1(0)$  band, cannot be measured because they are masked by other line broadening effects.

It should become obvious from the above description that the shape of the  $S_1(0)$  band is indeed the most informative part of the absorption spectrum of the Ar–HD van der Waals complex recorded and published thus far and a theoretical simulation of this shape is a task worth being undertaken. The line shape of the  $S_1(0)$  band will be simulated in this work by evaluation of the function  $\sigma^{\text{vdW}}(\omega)$ ,

$$\sigma^{\text{vdW}}(\omega) := \sigma_{\text{F} \leftarrow \text{B}}(\omega) + \sigma_{\text{F} \leftarrow \text{F}}^{\text{res}}(\omega), \quad (2)$$

which includes all the bound-free terms of the cross section of Eq. (1) and part of the free-free terms associated with the relevant shape resonances.

In the next part of this section, the line shape  $\sigma^{\text{vdW}}(\omega)$  will be expressed in terms of the reduced phototransition amplitudes which are quantities directly amenable to numerical treatment. For this purpose, it is necessary to introduce some elements of the quantum description of the dynamics for nonreactive atom-diatom systems (cf. Refs. 54–56). Although there will be nothing really specific to Ar–HD, explicit reference to this system will be done in order to prepare simultaneously the discussion of the next section.

Let configuration of the nuclei in the Ar–HD complex be described by the Jacobi coordinates in the space-fixed reference frame,  $\mathbf{r} := (r, \hat{\mathbf{r}})$ ,  $\mathbf{R} := (R, \hat{\mathbf{R}})$ , i.e., by the lengths and spherical angles of the vectors pointing from the H to D nucleus and from the nuclear center-of-mass of the diatom to the argon atom, respectively. Let  $H$  be the Hamiltonian governing the relative nuclear motion in the complex,

$$H = H_{\text{H-D}} + H_{\text{Ar-HD}}, \quad (3)$$

$$H_\alpha = K_\alpha + V_\alpha \quad \text{for } \alpha = \text{H-D, Ar-HD},$$

with  $K$  and  $V$  denoting the kinetic and potential energy operators for the indicated intra- and intermolecular modes of the motion. In the Jacobi coordinates, the kinetic energy operator for the intermolecular motion assumes the (simplest) form,  $K_{\text{Ar-HD}}(\mathbf{R}) = (1/2\mu)\hat{p}^2(R) + (1/2\mu R^2)\hat{\mathbf{I}}^2(\hat{\mathbf{R}})$ , where  $\hat{p}$  and  $\hat{\mathbf{I}}$  denote, respectively, the radial and angular momenta

operators, and  $\mu$  is the appropriate reduced mass. Similar expression for  $K_{H-D}(\mathbf{r})$  involves the operators  $\hat{p}(r)$  and  $\hat{\mathbf{j}}(\hat{\mathbf{r}})$ , and the diatomic reduced mass  $\mu_{H-D}$ .

To specify the continuum states of the Ar–HD complex, or the scattering states of  $H$ , one uses the splitting

$$H = H_0 + \bar{V}, \quad H_0 = H_{H-D} + K_{Ar-HD}, \quad (4)$$

where  $H_0$  is the Hamiltonian of the complex with noninteracting (infinitely separated) subunits and  $\bar{V} := V_{Ar-HD}$ . Let  $|E\hat{\mathbf{k}}_i(vjm_j)_i\rangle$ ,  $i = 1, \dots, \mathcal{N}$ , denote states of  $H_0$  of energy  $E$ ;  $\eta := (v, j, m_j)$  is the collection of quantum numbers characterizing the eigenstates of  $H_{H-D}$ ,  $H_{H-D}|\eta\rangle = \varepsilon_{vj}|\eta\rangle$ , and of  $\hat{J}_z$ ;  $|E\hat{\mathbf{k}}_i\rangle$  is the energy-normalized plane-wave eigenstate of  $K_{Ar-HD}$  with  $\hat{\mathbf{k}}_i$  denoting the direction of the wave-vector  $\mathbf{k}_i(E)$  and  $k_i^2(E) = (2\mu/\hbar^2)(E - \varepsilon_{(vj)})$ .  $\mathcal{N} = \mathcal{N}(E)$  denotes the number of states  $|\eta\rangle$  associated with open scattering channels identified by the  $(vj)$ -quantum numbers, for which  $k_i^2(E) > 0$ . The scattering states of energy  $E$ , denoted by  $|E^\pm, \hat{\mathbf{k}}_i(vjm_j)_i\rangle$  with the symbols “+” and “-” referring to outgoing and ingoing waves, respectively, and  $i = 1, \dots, \mathcal{N}$ , are (formally) defined as the states evolved from  $|E\hat{\mathbf{k}}_i(vjm_j)_i\rangle$  under the action of the Møller wave operators.<sup>55</sup> Obviously, the symbols behind the comma in  $|E^\pm, \hat{\mathbf{k}}_i(vjm_j)_i\rangle$  only indicate the state of the complex before the interaction. Neither  $\hat{\mathbf{k}}$  nor any of the  $\eta$ -numbers are (strictly) preserved by  $\bar{V}$ . The probability amplitude to find the complex in a state  $|E\hat{\mathbf{k}}_f(vjm_j)_f\rangle$  after the interaction is given by the respective element of the  $\mathbf{S}$ -matrix,  $S_{j,i}(E) = \delta_{j,i} - 2\pi i \langle E\hat{\mathbf{k}}_f\eta_f | V | E^+, \hat{\mathbf{k}}_i\eta_i \rangle$ .

Due to rotational and reflection invariance of the Hamiltonian  $H$ , the scattering states  $|E^\pm, \hat{\mathbf{k}}_i v j m_j\rangle$  can be disintegrated into partial states  $|E^\pm J M p, v j l\rangle$  with definite quantum numbers of  $\hat{\mathbf{J}}^2 = (\hat{\mathbf{j}} + \hat{\mathbf{I}})^2$  and  $\hat{J}_z$ , and spectroscopic parity  $p$ ,  $p := (-1)^{j+l+J}$ ,

$$|E^\pm, \hat{\mathbf{k}}_i v j m_j\rangle = \sum_{JM} \sum_{p=\pm 1} \sum_{l(p)} |E^\pm J M p, v j l\rangle \times \sum_{m_l} i^l C(jlJ, m_j m_l M) Y_{lm_l}^*(\hat{\mathbf{k}}_i), \quad (5)$$

where  $l(p) = |J - j| + 2\lambda - \lambda_{\min}(p)$  for  $\lambda = \lambda_{\min}, \lambda_{\min} + 1, \dots, \lambda_{\max}$ , with  $\lambda_{\min} = (1 - p/2)$  and  $\lambda_{\max} = \min(J, j)$ ,  $C(\dots, \dots)$  denotes the Clebsch-Gordan coefficient, and  $Y$ , the normalized spherical harmonics. Correspondingly, the  $\mathbf{S}$ -matrix can be disintegrated into partial matrices  $\mathbf{S}^p$ , which describe the  $\gamma_i \rightarrow \gamma_f$  transitions in the complex for  $i, f = 1, \dots, N^o$ , where  $\gamma := (vj l)$  and  $N^o = N^o(E, J, p)$  is the number of the open  $\gamma$ -states for a given  $J$  and  $p$ .

Energies,  $E_n^{\text{res}}$ , and widths,  $\Gamma_n$ , or decay-times,  $\tau_n = \hbar/2\Gamma_n$ , of the metastable states of Ar–HD can most precisely be defined by their relation to the poles  $\mathcal{E}_n$  of the Green's operator  $G(\mathcal{E}) := (\mathcal{E} - H)^{-1}$  in the fourth quadrant of the complex energy plane (assuming that the continuum spectrum of  $H$  begins at 0), namely,  $\mathcal{E}_n := E_n^{\text{res}} - i\Gamma_n/2$ . Of interest here are, of course, not so much the precise positions of these resonance poles as it is the way they influence the

scattering states of  $H$  in the nearby range of  $E$ . Sufficiently (if not extremely) accurate information can be extracted from the energy dependence of the partial  $\mathbf{S}$ -matrices<sup>57–58</sup> or other suitable quantities directly related to them.<sup>59–61</sup> In the present study the collision lifetime matrices,  $\mathbf{Q}^{Jp}(E) = i\hbar(d/dE)\mathbf{S}^{Jp}(E)^\dagger\mathbf{S}^{Jp}(E)$ , are analyzed and the resonance energies and widths are determined as parameters of the Breit–Wigner formula fitted to traces of these matrices,  $\text{Tr}\mathbf{Q}^{Jp}(E) \approx \hbar\Gamma_n / [(E - E_n^{\text{res}})^2 + (\Gamma_n/2)^2]$ , for  $E$  in the vicinity of  $E_n^{\text{res}}$ . (Actually, a more refined parametrization will be used, cf. Sec. IV.)

Bound states of the Ar–HD complex can also be associated with the poles of the Green's operator  $G(\mathcal{E})$ , but occurring on the real negative axis of the  $\mathcal{E}$ -plane, i.e.,  $-|\mathcal{E}_n| = \mathcal{E}_n := E_n^B$ . They will be denoted by  $|E^B J p\rangle_n M_n$ .

Returning to the photoabsorption line shape formula (1), one should identify the  $|f\rangle$ -ket with one of the ingoing-wave states at the energy  $E = E_f$ , i.e.,  $|f\rangle := |E_f^-, \hat{\mathbf{k}}_f \eta_f\rangle$ ,  $f = 1, \dots, \mathcal{N}(E_f)$ . Therefore,  $\Sigma_f := \int dE_f \int d\hat{\mathbf{k}}_f \Sigma_{\eta_f}$ . In the free-free cases,  $|i\rangle := |E_i^+, \hat{\mathbf{k}}_i \eta_i\rangle$ ,  $i = 1, \dots, \mathcal{N}(E_i)$ , and the meaning of  $\Sigma_i$  is analogous to the above. The Boltzmann factor assumes the form,  $P_i = (1/Z) e^{-\beta e_i} P_{\eta_i} = (1/Z) e^{-\beta e_i / \sum_{k=1}^{\mathcal{N}(E_i)} e^{-\beta e_{(vj)k}}} = P(E_i)$ , where  $e_i := E_i - \varepsilon_{(vj)_i}$  is the translational energy,  $\beta = k_B T$ , and  $Z$  denotes the sum of the states of relative motion of the complex. By expanding the initial and final states into partial waves according to Eq. (5) and exploiting the orthogonality properties of the Clebsch–Gordan coefficients and spherical harmonics, one derives

$$\begin{aligned} & \sum_{m_j} \sum_{m_i} \int d\hat{\mathbf{k}}_f \int d\hat{\mathbf{k}}_i | \langle f | \boldsymbol{\epsilon} \cdot \bar{\mathbf{d}} | i \rangle |^2 \\ &= \sum_{qq} (-1)^{\bar{q}+q} \boldsymbol{\epsilon}_{-q}^* \boldsymbol{\epsilon}_{-q} \\ & \times \sum_{J_f M_f} \sum_{J_i M_i} \sum_{p_f p_i} \sum_{l(p_f) l(p_i)} \langle \dots | \bar{d}_q | \dots \rangle^* \\ & \times \langle E_f^- J_f M_f p_f, \gamma_f | \bar{d}_q | E_i^+ J_i M_i p_i, \gamma_i \rangle, \end{aligned}$$

where  $\boldsymbol{\epsilon}_q$  and  $\bar{d}_q$ ,  $q = -1, 0, 1$ , denote the spherical components of the respective vectors. By applying the Wigner–Eckart theorem,<sup>62</sup>

$$\begin{aligned} & \langle E_f^- J_f M_f p_f, \gamma_f | \bar{d}_q | E_i^+ J_i M_i p_i, \gamma_i \rangle \\ &= C(J_i 1 J_f, M_i q M_f) \langle E_f^- J_f p_f, \gamma_f | \bar{\mathbf{d}} | E_i^+ J_i p_i, \gamma_i \rangle, \end{aligned}$$

one obtains the following formula for the free-free contribution to the absorption spectrum,

$$\begin{aligned} \sigma_{F \leftarrow F}(\omega) &= \frac{4\pi^2 \omega}{3c} \int dE_i P(E_i) \sum_{J_f} \sum_{J_i p_i} \delta(J_f 1 J_i) \\ & \times \text{Tr} \mathbf{T}_{F \leftarrow F}^\dagger \mathbf{T}_{F \leftarrow F}(\omega; J_f J_i p_i E_i), \quad (6) \end{aligned}$$

where  $\delta(J_f 1 J_i)$  stands for the triangular condition  $|J_f - J_i| \leq 1$ , and the matrix  $\mathbf{T}_{F \leftarrow F}(\omega; J_f J_i p_i E_i)$  is built of the reduced free-free phototransitions amplitudes,

$$(\mathbf{T}_{F \leftarrow F})_{\gamma_f, \gamma_i} := \sqrt{2J_f + 1} \langle E_f^- J_f p_f, \gamma_f | \bar{\mathbf{d}} | E_i^+ J_i p_i, \gamma_i \rangle$$

with  $E_f = E_i + \hbar \omega$ ,

$$p_f = (-1)^{J_f + J_i + 1} p_i,$$

for  $i = 1, \dots, N_i^o$  and  $f = 1, \dots, N_f^o$ , where  $N_i^o := N^o(E_i, J_i, p_i)$  and  $N_f^o := N^o(E_f, J_f, p_f)$ . The superscript ‘‘res’’ added to  $\sigma_{F \leftarrow F}$  in Eq. (2) means that the summation over  $J_i$  in the above formula is restricted to those terms for which the related lifetime matrices,  $\mathbf{Q}^{J_i p_i}(E_i)$  and  $\mathbf{Q}^{J_f p_f}(E_i + \hbar \omega)$ , reveal sufficiently large collision times in some regions of  $E_i \in [0, \infty]$  and in some regions of  $\omega$  within the investigated range of light frequency.

For the bound-free cases we have  $|i\rangle := |(E^B J p)_i M_i\rangle$ ,  $\Sigma_i := \Sigma_i \Sigma_{M_i}$ , and  $P_i = (1/Z) e^{-\beta E_i^B} := P_i$ . Repeating all the steps of the above derivation, except for the partial-wave expansion of the initial state, one obtains

$$\begin{aligned} \sigma_{F \leftarrow B}(\omega) &= \frac{4\pi^2 \omega}{3c} \sum_i P_i \sum_{J_f} \delta(J_f 1 J_i) \mathbf{T}_{F \leftarrow B}^\dagger \mathbf{T}_{F \leftarrow B}(\omega; J_f J_i p_i E_i^B) \\ &= \sum_i (2J_i + 1) P_i \sigma^{\text{tot}}(\omega; (E^B J p)_i), \end{aligned} \quad (7)$$

where  $\mathbf{T}_{F \leftarrow B}$  denotes the  $N_i^o$ -dimensional vector of the reduced photodissociation amplitudes,

$$(\mathbf{T}_{F \leftarrow B})_{\gamma_f} := \sqrt{2J_f + 1} \langle E_f^- J_f p_f, \gamma_f | \bar{\mathbf{d}} | E_i^B J_i p_i \rangle$$

with  $E_f = E_i^B + \hbar \omega$ .

Here  $p_f$  is related to  $p_i$  as in the free-free amplitudes and  $\sigma^{\text{tot}}$  is the total cross section for photodissociation of the Ar–HD molecule from its  $(E^B J p)_i$ -energy level averaged over the magnetic sublevels. Finally, the reduced phototransition amplitudes have to be specified,

$$\begin{aligned} \langle E_f^- J_f p_f, \gamma_f | \bar{\mathbf{d}} | E_i^+ J_i p_i, \gamma_i \rangle &= \int dR \sum_{s,k} F_{\gamma_s}^{(+)} J_f p_f(E_f \gamma_f; R) D_{\gamma_s, \gamma_k} \\ &\quad \times (J_f p_f J_i p_i; R) F_{\gamma_k}^{(+)} J_i p_i(E_i \gamma_i; R) \\ &:= (\mathbf{F}^{(-) J_f p_f}(E_f \gamma_f) | \mathbf{D}(J_f p_f J_i p_i) \mathbf{F}^{(+)} J_i p_i(E_i \gamma_i)), \end{aligned} \quad (8)$$

$$\begin{aligned} \langle E_f^- J_f p_f, \gamma_f | \bar{\mathbf{d}} | E_i^B J_i p_i \rangle &= (\mathbf{F}^{(-) J_f p_f}(E_f \gamma_f) | \mathbf{D}(J_f p_f J_i p_i) \mathbf{F}^{(B) J_i p_i}(E_i^B)), \end{aligned}$$

where  $D_{\gamma_s, \gamma_k}(J_f p_f J_i p_i; R) := \int dr \chi_{(v_j)_s}(r) [(4\pi/\sqrt{3}) \Sigma_{\bar{L}\bar{A}} \bar{d}_{\bar{L}\bar{A}} \times (r, R) \langle j_s l_s J_f p_f | \mathcal{Y}_{\bar{L}\bar{A}}^1 | j_k l_k J_i p_i \rangle] \chi_{(v_j)_k}(r)$ . In these formulas, the (vectors of) functions  $\mathbf{F}^{(+)} J p(E \gamma; R)$  and  $\mathbf{F}^{(-)} = (\mathbf{F}^{(+)})^*$  are the standard representation of the atom-diatom scattering waves,

$$\begin{aligned} \langle \mathbf{r}, \mathbf{R} | E^\pm J M p, \gamma \rangle &= \frac{1}{R} \sum_{k=1}^N F_{\gamma_k}^{(\pm) J p}(E \gamma; R) \\ &\quad \times \frac{1}{r} \chi_{(v_j)_k}(r) \mathcal{Y}_{(j_l)_k}^{J M p}(\hat{\mathbf{r}}, \hat{\mathbf{R}}), \end{aligned} \quad (9)$$

in the basis  $\Phi^{J M p}(\mathbf{r}, \hat{\mathbf{R}}) := \{ (1/r) \chi_{(v_j)_k}(r) \mathcal{Y}_{(j_l)_k}^{J M p}(\hat{\mathbf{r}}, \hat{\mathbf{R}}) \}$  built of eigenfunctions of  $H_{H-D}$ ,  $\hat{\mathbf{J}}^2$ ,  $\hat{J}_z$ , and  $\hat{P}$  (the parity operator),  $\chi_{v_j}(r)$  denotes the radial ro-vibrational function of the diatom, and  $\mathcal{Y}_{j_l}^{J M p}(\hat{\mathbf{r}}, \hat{\mathbf{R}})$ , the Clebsch-Gordan coupled product of spherical harmonics (the bipolar harmonics<sup>63</sup>) of parity  $p$ . Since all open  $(v_j)$ -channels should be present in the basis,  $N > N^o$ .  $\mathbf{F}^{(B)}$  denotes the representation of the Ar–HD bound states in the same basis. The matrix  $\mathbf{D}(J_f p_f J_i p_i; R)$  represents the induced-dipole operator,  $\bar{d}_q(\mathbf{r}, \mathbf{R})$ ; the coefficients  $\langle \dots | \mathcal{Y}_{\bar{L}\bar{A}}^1 | \dots \rangle$  are the reduced matrix elements arising from the integrals  $\int d\hat{\mathbf{r}} f d\hat{\mathbf{R}} (\mathcal{Y}_{j_s l_s}^{J_f M_f p_f})^* \mathcal{Y}_{\bar{L}\bar{A}}^{l_q 1} \mathcal{Y}_{j_k l_k}^{J_i M_i p_i}$ . Explicit formulas for these elements in terms of the  $3-j$  and  $6-j$  coefficients are listed, e.g., in Ref. 11.

The radial functions  $\mathbf{F}^{(B) J_i p_i}(E_i^B; R)$  and  $\mathbf{F}^{(+)} J p(E; R) := \{ \mathbf{F}^{(+)} J p(E, \gamma_i; R) \}$ ,  $i = 1, \dots, N^o$  satisfy the equation

$$[\mathbf{E} \mathbf{I} - \mathbf{H}^{J p}(R)] \mathbf{F}^{(\alpha) J p}(E; R) = \mathbf{0}, \quad \alpha = +, B, \quad (10)$$

where  $\mathbf{H}^{J p} = \mathbf{H}_0^{J p} + \mathbf{V}^{J p}$  denotes the representation of the Hamiltonian  $H$  in the basis  $\Phi^{J M p}$ ,  $\mathbf{H}_0^{J p}$  is a diagonal matrix,  $\mathbf{H}_0^{J p}(R) = (1/2\mu) (\mathbf{p}_R^2 + (\hbar^2 \mathbf{I}^{J p}/R^2)) + \varepsilon$  with  $(\mathbf{p}_R)_{i,j} = -i\hbar \delta_{i,j} (d/dR)$  and with  $\mathbf{I}^{J p}$  and  $\varepsilon$  involving the respective numbers  $l(l+1)$  and the energies  $\varepsilon_{v_j}$ ,  $\mathbf{V}^{J p}(R)$  is the potential coupling matrix. The radial functions vanish at  $R = 0$ . For  $R \rightarrow \infty$ , the functions  $\mathbf{F}^{(B) J_i p_i}(E_i^B; R)$  decay exponentially and

$$\mathbf{F}^{(+)} J p(E; R) \xrightarrow{R \rightarrow \infty} \frac{l}{\sqrt{2\pi\hbar}} [\mathbf{O}^{-J p}(R) - \mathbf{O}^{+J p}(R) \mathbf{S}^{J p}], \quad (11)$$

where  $\mathbf{O}^{+J p}$  and  $\mathbf{O}^{-J p} = (\mathbf{O}^{+J p})^*$  denote  $N \times N^o$  blocks of the  $N \times N$  diagonal matrices  $\tilde{\mathbf{O}}^{\pm J p}$ ,  $[\tilde{\mathbf{O}}^{\pm J p}(R)]_{f,i} = \delta_{f,i} \sqrt{(\mu/\hbar k_f)} \mathcal{H}_{l_f}^{\pm}(k_f R)$ , and  $\mathcal{H}_{l_f}^{\pm}$  are the spherical Riccati-Hankel functions of the  $l_f$ th order with  $l_f = l_f(J, p, j_f)$ .

Having introduced in the above description of workable formulas for the phototransition amplitudes the representation of the atom-diatom dynamics in terms of the radial Hamiltonian matrix and vectors of radial functions, one can add some information on the determination of other relevant quantities in this representation. (The indices  $J$  and  $p$  will be omitted throughout the rest of this section.) To determine the energies and widths of metastable states, it is convenient to use the following formula for the lifetime matrix  $\mathbf{Q}$ ,

$$\begin{aligned} \mathbf{Q} &= 2\pi\hbar (\mathbf{F}^{(+)} | P_{[0, R_\infty]} \mathbf{F}^{(+)} \\ &\quad - i\hbar (\mathbf{O}_E^- - \mathbf{O}_E^+ \mathbf{S} | \mathbf{C}(R_\infty) (\mathbf{O}^- - \mathbf{O}^+ \mathbf{S})), \end{aligned} \quad (12)$$

where the subscript  $E$  denotes the derivative with respect to the energy,  $P_{[0, R_\infty]}$  is the projector on the interval  $[0, R_\infty]$  of the  $R$ -coordinate outside which the interaction  $\bar{V}$  is practically negligible, and  $\mathbf{C}(R_\infty)$  is the operator of the probability flux through the surface  $R = R_\infty$ ,  $\mathbf{C}(R_\infty) := (1/2\mu) [\delta(R$

$-R_\infty)\mathbf{p}_R + \mathbf{p}_R\delta(R-R_\infty)]$ . The first term of this formula has the meaning of the time the atom-diatom system spends within the region of the configuration space bounded by the surface  $R=R_\infty$  while the second term gives roughly the time the system would spend in the same region if there were no interactions between the subunits (cf. Ref. 53). Since from the standpoint of the scattering theory, a predissociating state, or a Feshbach resonance, is viewed as a temporal conversion into internal excitation of the entire translational energy (available to the system at infinite separation of the subunits) or as a quasi-bound state embedded into a submanifold of closed scattering channels, say  $C_{\text{res}}$ , the above formula suggests that the following term of  $\mathbf{Q}$  should contain the information on the energy and width of such a state, or on the position of the resonance pole,

$$\mathbf{Q}_{\text{res}} = 2\pi\hbar(\mathbf{F}^{(+)}|\mathbf{P}_{\text{res}}P_{[0,R_\infty]}\mathbf{F}^{(+)}), \quad (13)$$

where  $\mathbf{P}_{\text{res}}$  denotes the projector on the components of  $\mathbf{F}^{(+)}$  connected with the channels in  $C_{\text{res}}$ . Fitting the Breit-Wigner formula to this term only, strictly, to  $\text{Tr}\mathbf{Q}_{\text{res}}(E)$  at  $E \approx E_n^{\text{res}}$ , is believed to give a better chance for extracting the true position of the resonance pole. It should be noted that the diagonal elements of this resonance part of the lifetime matrix, strictly the quantities  $(1/2\pi\hbar)(\mathbf{Q}_{\text{res}})_{ii}$ ,  $i = 1, \dots, N^o$ , coincide with the ‘‘amplitudes’’ considered by Dalgarno and co-workers in their method for multichannel resonances.<sup>64,65</sup>

The bound state energies of the atom-diatom complex can be determined as poles of the following function:<sup>66</sup>

$$T^{\text{ar}}(E) := (\mathbf{F}^{\text{ar}}|\mathbf{G}(E)\mathbf{F}^{\text{ar}}), \quad (14)$$

where  $\mathbf{G}$  denotes the matrix radial Green’s function,  $[\mathbf{E}\mathbf{I} - \mathbf{H}(R)]\mathbf{G}(R; \bar{R}) = \delta(R - \bar{R})$ , which vanishes at both ends of the interval  $[0, R_\infty]$  and  $\mathbf{F}^{\text{ar}}$  is a vector of radial functions that have a non-negligible overlap with the true eigenfunction of the state sought for, otherwise arbitrary. This way of determination of bound state energies from the coupled radial equations resembles the well-known artificial channel method<sup>67,68</sup> and, actually, is a simplification of this method. (A detailed discussion will be given in a future publication.)

In the above outline, all the elements of the atom-diatom dynamics involved in the photoabsorption process have been specified within the most accurate approach—the close-coupling approximation in the basis that accounts for the vibrational and rotational inelasticity, i.e., for the mixing of the diatomic states with different  $v$  and  $j$  by the interaction with the atom. However, investigations of the dynamics of the atom-diatom van der Waals complexes rarely require such an accuracy. Because of the weakness of the binding of these complexes, the vibrational inelasticity is very small. A manifestation of this fact is the disparity between the rates of the vibrational and rotational predissociation in the Ar–HD complex, already mentioned in the first part of this section. Calculations aimed at the estimation of the size of this disparity were the only part of this work where the general expansions, Eq. (9), were necessary. Bases with fixed  $v$ -number were applied in all other calculations.

### III. DYNAMICS OF THE Ar–HD COMPLEX

As mentioned in the Introduction, the dynamics of atom-diatom van der Waals complexes, and especially of the complexes formed by the hydrogen molecule and its isotopes with rare gas atoms, has been the subject of intensive theoretical investigations inspired by the experimental discovery of Kudian *et al.* in 1965 and by later measurements of McKellar and Welsh. The knowledge accumulated over the years, in particular on the correlation between the observed patterns of spectral lines and the anisotropy of intermolecular interactions, has been systematized in a number of review articles (two of the latest are Refs. 69 and 70). The complexes have been categorized according to the relative strength of the coupling between the intramolecular and intermolecular modes of the rotational motion and for each of the three categories (cases) distinguished an appropriate angular momentum coupling scheme (or angular basis set) has been indicated which allows us to introduce some nearly conserved quantum numbers to assign the energy levels. The Ar–HD complex belongs to the weak-anisotropy category (case (a) of the Bratoz and Martin classification<sup>71</sup>) for which  $j$  and  $l$  are nearly good angular momentum quantum numbers. Together with the well preserved diatomic vibrational quantum number, this gives a set of five quantum numbers— $(\bar{v}, \bar{J}, n, \bar{l}, J)$  with the bar marking hereafter the approximate ones—to assign the individual bound or metastable states of the complex. (The exact parity quantum number,  $p$ , is determined, of course, by  $\bar{J}$ ,  $\bar{l}$ , and  $J$ .) The numbers are written in a sequence that shows the ordering of the states according to their energy. The very nature of a van der Waals complex is reflected in that the energy levels separate into groups which can be labeled with the quantum numbers related to the intramolecular vibrational and rotational motions,  $\bar{v}$  and  $\bar{J}$ . The quantum number  $n$  is connected with intermolecular vibrations, i.e., with the radial motion of the ‘‘reduced atom’’—the particle of the reduced mass  $\mu$ —which is bound within the van der Waals well of the (effective radial) intermolecular potential or temporarily bound behind the centrifugal barrier arising from the rotations of the ‘‘reduced atom’’ around the center-of-mass of HD. Most closely spaced in energy are the states which differ only in the value of the total angular momentum  $J$ ; this is just the primary sign of weakness of anisotropy of the Ar–HD potential.

The intermolecular potential for Ar–HD is related to the potential for Ar–H<sub>2</sub>, denoted hereafter by  $V$ , through the coordinate transformation which accounts for the shift of the diatom center-of-mass,<sup>72</sup>  $\bar{V}(\mathbf{r}, \mathbf{R}) := V(\mathbf{r}, \mathbf{R} + f\mathbf{r})$ , where  $f = m_D/(m_H + m_D) - \frac{1}{2} \approx \frac{1}{6}$ . In the standard representation  $V$  is given by an expansion in terms of Legendre polynomials and the coefficients of this expansion, the functions  $V_L(r, R)$ , are given by expansions in powers of the relative displacement of the  $r$ -distance from its mean value  $r_0$  in the ground rovibrational state of H<sub>2</sub>,

$$V(\mathbf{r}, \mathbf{R}) = \sum_{L=0,2,\dots}^{L_{\max}} V_L(r, R) P_L(\cos(\hat{\mathbf{r}} \cdot \hat{\mathbf{R}})), \quad (15)$$

$$V_L(r, R) = \sum_{k=0}^{k_{\max}} V_{L,k}(R) \zeta^k,$$

where  $\zeta := (r/r_0) - 1$ . The anisotropy of the potential is characterized by the orders  $L$  of the terms occurring in expansion (15) and by their strengths determined by the coefficient functions  $V_L$ . While only even order anisotropy terms contribute to the potential  $V$ , both even and odd orders anisotropies arise in the transformed potential  $\bar{V}$ . For accurate determination of the respective strength functions, denoted by  $\bar{V}_L(r, R)$ , the expansion of  $\bar{V}(\mathbf{r}, \mathbf{R})$  in Legendre polynomials has to be done numerically.<sup>69,72</sup>

Obviously, not only the properties of the intermolecular potential but also the anisotropy of the induced dipole moments of the complexes are reflected in the observed spectra. Modeling of the induced dipoles is an important part of the theoretical research on the absorption of rare gas atom-hydrogen molecule systems, although it has been done primarily for the simulation of the shape of the collision-induced parts of the spectra.<sup>52</sup> The only models which have arisen from investigations of van der Waals spectra of these systems are those published by Dunker and Gordon, Ref. 11, and the refined version proposed by Hutson.<sup>73</sup> The induced dipole moment function for Ar-HD is related to the function  $\mathbf{d}(\mathbf{r}, \mathbf{R})$  for Ar-H<sub>2</sub> the same way as the intermolecular potential,  $\bar{\mathbf{d}}(\mathbf{r}, \mathbf{R}) := \mathbf{d}(\mathbf{r}, \mathbf{R} + \mathbf{r})$ . Obviously, differently coupled spherical harmonics have to be used to represent the angular dependence of these functions. The appropriate representation of  $\bar{d}_q(\mathbf{r}, \mathbf{R})$  (which has already been exploited in Sec. II) reads

$$\bar{d}_q(\mathbf{r}, \mathbf{R}) = \frac{4\pi}{\sqrt{3}} \sum_{\bar{L}\bar{A}} \bar{d}_{\bar{L}\bar{A}}(r, R) \mathcal{Y}_{\bar{L}\bar{A}}^{1q1}(\hat{\mathbf{r}}, \hat{\mathbf{R}}). \quad (16)$$

The coefficients of this expansion, i.e., the functions  $\bar{d}_{\bar{L}\bar{A}}(r, R)$ ,  $\bar{L}=0,1,\dots$ , can be generated from the coefficients  $d_{L\Lambda}(r, R)$ ,  $L=0,2,\dots$ , of the expansion for  $d_q(\mathbf{r}, \mathbf{R})$ . See the Appendix for a brief sketch of the derivation of the expression for  $\bar{d}_{\bar{L}\bar{A}}(r, R)$ .

The observed transitions between the states of the Ar-HD complex and the notation used for their assignment are as follows.  $Q_{\bar{v}}(\bar{J})$  and  $S_{\bar{v}}(\bar{J})$  denote the  $(0, \bar{J}) \rightarrow (\bar{v}, \bar{J})$  and  $(0, \bar{J}) \rightarrow (\bar{v}, \bar{J}+2)$  bands of transitions, respectively. The branches of these bands related to the transitions  $\bar{I} \rightarrow \bar{I} + \Delta\bar{I}$  with  $\Delta\bar{I} = +1, -1, +3, -3$  (the two latter not occurring in the  $Q_{\bar{v}}(0)$  band) are conventionally denoted by  $R$ ,  $P$ ,  $T$ , and  $N$ , respectively. Further splitting of the branches may arise from the allowed  $J \rightarrow J+1, J-1, J$  transitions. The subscripts “+,” “-,” and “0,” respectively, will be added to the  $R$  and  $P$  symbols to denote these subbranches in the  $S_1(0)$  and in the  $Q_1(1)$  bands. To denote individual transitions within branches or subbranches the  $\bar{I}$ -number of the initial states will be shown in parentheses. For transitions originating from the states with  $\bar{J} > 0$ , the  $J$ -value of the state will be

added for uniqueness. For instance, the symbol  $R_-(\bar{I})$  will denote the  $(\bar{I}, J=\bar{I}) \rightarrow (\bar{I}+1, \bar{I}-1)$  transition in the  $S_1(0)$  band and  $R_-(\bar{I}, J)$  with  $J=\bar{I}$ —the same transition in the  $Q_1(1)$  band. When the excitation of the van der Waals stretch is involved, the initial ( $n''$ ) and final ( $n'$ ) values of the  $n$ -number will also be shown in the parentheses after semicolon, e.g.,  $R_-(\bar{I}; n'', n')$ . In the  $Q_1(1)$  band, the most complex of the bands studied in this work, there is one  $P_+$  subbranch consisting of transitions  $P_+(\bar{I}, J=\bar{I}-1)$  for  $\bar{I}=1, \dots$ , and one  $R_-$  subbranch of transitions  $R_-(\bar{I}, J=\bar{I}+1)$  for  $\bar{I}=0, \dots$ , but two  $P_0$  and  $R_0$  subbranches corresponding to transitions from  $(\bar{I}, J)$  with  $J=\bar{I}-1, \bar{I}$  and with  $J=\bar{I}, \bar{I}+1$ , respectively, and three  $P_-$  and  $R_+$  subbranches corresponding to all three possible  $J$  values in the initial states.

#### IV. SOME DETAILS ON CLOSE-COUPPLING CALCULATIONS

In the expansion of the wave functions for the bound and metastable states of the complex, Eq. (9), associated with a given Ar+HD( $\bar{v}, \bar{J}$ ) dissociation threshold, the following rovibrational  $(v, j)$ -states of HD were included:

- (i)  $(v=\bar{v}, j=0-j_{\max})$  and  $(v=\bar{v}, j=1-j_{\max})$  with  $j_{\max}=\bar{J}+2$  for the  $p=+1$  and  $p=-1$  parity states, respectively—when energies and widths due to the rotational predissociation and/or tunneling were calculated. In the simulation of the shape of the  $S_1(0)$  band the state  $(v=1, j=4)$  was omitted from the basis.
- (ii)  $(v=0, j=0-8; v=1, j=0-2)$ —when rates of the vibrational predissociation in the  $Q_1(0)$  band were evaluated.

The radial rovibrational functions of HD,  $\chi_{vj}(r)$ , were calculated from the recent potential of Ref. 74 (with adiabatic, radiative, and relativistic corrections included). The energies of the  $(v=0, 1, j=0-3)$  states were set equal to the most accurate theoretical values of Ref. 75, i.e., the nonadiabatic corrections have been added to the values obtained from the calculations of the functions  $\chi_{vj}(r)$ . Accurate values of  $\varepsilon_{\bar{v}\bar{J}}$  are actually necessary to obtain transition energies comparable with experiment. In the calculations for the HD subunit, the nuclear masses of H and D,  $m_p=1836.1527m_e$  and  $m_d=3670.4831m_e$ , respectively, were used. In the calculations on the entire complex, atomic masses were taken:  $m_{\text{Ar}}=39.9627u$ ,  $m_{\text{H}}=1.007825u$ ,  $m_{\text{D}}=2.0141009u$  ( $1u=1822.88867m_e$ ).

The potential coupling matrices  $\mathbf{V}^{JP}$  were constructed starting from the two potentials for Ar-H<sub>2</sub>: the SAPT potential of Ref. 37 and XC(fit) of Ref. 14. The maximal order of the Legendre polynomial included in the expansions of the resulting Ar-HD potentials  $\bar{V}$  was  $L=8$ . The matrices  $\mathbf{D}$  for the reduced phototransition amplitudes were constructed from the Dunker-Gordon model<sup>11</sup> of the induced dipole of Ar-H<sub>2</sub>. The highest component of the bispherical harmonics included in expansion (16) of the transformed dipole mo-

TABLE I. Convergence<sup>a</sup> of the energies and widths for selected ( $\bar{\nu}=1, \bar{J}=2, n=0, \bar{I}, J=\bar{I} \pm 2$ ) states of Ar–HD. Results are generated from the XC potential.<sup>b</sup>

$\bar{I}$	$J$	Tr $\mathbf{Q}$				Tr $\mathbf{Q}_{\text{res}}$			
		$E_0$	$\Gamma_0$	$E^{\text{res}}$	$\Gamma$	$E_0$	$\Gamma_0$	$E^{\text{res}}$	$\Gamma$
2	4	-24.041	0.675	-24.040	0.648	-24.040	0.651	-24.041	0.649
		-24.042				-24.042	0.651	-24.043	0.650
5	3	-15.039	0.607	-15.039	0.586	-15.040	0.587	-15.039	0.586
		-15.041				-15.041	0.586	-15.041	0.586
7	5	-5.367	0.437	-5.367	0.426	-5.368	0.427	-5.368	0.426
		-5.370				-5.370	0.426	-5.370	0.426
8	6	0.374	0.337	0.366	0.347				
		0.373	0.337	0.366	0.347				
10	8	12.956	0.687	12.958	0.659				
		12.957	0.685	12.958	0.658				

<sup>a</sup>Parameters obtained from the analysis of traces of  $\mathbf{Q}(E)$  and  $\mathbf{Q}_{\text{res}}(E)$  are compared for the Feshbach-type resonances.  $E_0$  and  $\Gamma_0$  were obtained from fitting to the Breit–Wigner formula;  $E^{\text{res}}$  and  $\Gamma$ , to Eq. (17). Both the energies and widths are given in  $\text{cm}^{-1}$ ; the energies are relative to the  $\varepsilon_{12}$ -threshold, see Table II.

<sup>b</sup>The upper entries were computed in the basis with ( $\nu=1, j=0-3$ ); the lower, in the basis with the  $j=4$  state included.

ment function  $\bar{d}_q$  was  $\bar{L}=5, \bar{\Lambda}=4$ . The largest sets of the coupled radial Eqs. (10) constructed in bases (i) and (ii) consisted of 15 and 51 equations, respectively. The following quantities involving solutions of the radial equations were directly evaluated:

- (1) The function  $T^{\text{ar}}(E)$ , Eq. (14), used to determine the bound state energies;
- (2) The bound state functions  $\mathbf{F}^{(B)}(R)$  used as input to evaluate the photodissociation amplitudes;
- (3) The lifetime matrices  $\mathbf{Q}$  and  $\mathbf{Q}_{\text{res}}$ , Eqs. (12) and (13), used to determine the energies and widths of metastable states;
- (4) The photodissociation amplitudes  $\mathbf{T}_{\text{F} \leftarrow \text{B}}(\omega; J_f J_i p_i E_i^B)$ , Eq. (7), necessary to simulate the shape of the  $S_1(0)$  band. Each of 29 of these amplitudes was evaluated at ca. 1000 photon energies covering the range 3865–3906  $\text{cm}^{-1}$ ;
- (5) The free-free phototransition amplitudes  $\mathbf{T}_{\text{F} \leftarrow \text{F}}(\omega; J_f J_i p_i E_i)$ , Eq. (6), from the  $p_i=1$  states with  $J_i=8-12$ . These 15 amplitudes were found to contribute significantly to the simulated shape. They were evaluated typically at 120–150 photon energies from the range given above and at 180–200 values of  $E_i$  in the range 0–360  $\text{cm}^{-1}$ . (Interpolation was used in order to calculate the integrals over  $E_i$ .)

All these quantities were evaluated numerically with the help of an appropriate version of the  $\mathcal{L}$ -matrix propagation (generalized log-derivative) method.<sup>46,66,76</sup> This method is particularly advantageous for the evaluation of the free-free phototransition amplitudes and of all the other integrals involving multichannel scattering functions (e.g.,  $\mathbf{Q}_{\text{res}}$ ). Direct evaluation of these functions was avoided (without introducing any artificial channel, cf. Refs. 65,67), and their accuracy, even in the presence of closed channels, was assured. The values of  $R_\infty$  were close to 40 Å and 20 Å in the calculations of the continuum and bound states, respectively, and all integrations were carried out with a step size of 0.01 Å.

Finally, more details should be given on how the reso-

nance energies and widths have been extracted from the quantities calculated,  $\text{Tr } \mathbf{Q}^{JP}(E)$  and  $\text{Tr } \mathbf{Q}_{\text{res}}^{JP}(E)$ . As already stated, the matrices  $\mathbf{Q}_{\text{res}}^{JP}$  were designed for the detection of Feshbach-type resonances only; they were evaluated with the projector  $\mathbf{P}_{\text{res}} = \mathbf{P}_{\bar{\nu}\bar{J}\bar{I}}$ , where  $\mathbf{P}_{\bar{\nu}\bar{J}\bar{I}}$  denotes a matrix with only one nonzero element,  $(\mathbf{P}_{\bar{\nu}\bar{J}\bar{I}})_{\bar{k}, \bar{k}} = 1$ , where  $\bar{k}$  is the index of the function in the basis  $\Phi^{JM_p}$  with  $(\nu j l)_{\bar{k}} = (\bar{\nu} \bar{J} \bar{I})$ , cf. Eq. (9). The procedure started with the determination of the maximum,  $E_0$ , of the ( $n$ th) resonance structure in the function  $\text{Tr } \mathbf{Q}_{\text{res}}^{JP}(E)$  (or  $\text{Tr } \mathbf{Q}^{JP}(E)$ ). This gave a first estimate of the energy of the  $(\bar{\nu} \bar{J} n \bar{I} J)$  metastable state. The corresponding estimate of the width was calculated from  $\Gamma_0 = (4\hbar / \text{Tr } \mathbf{Q}_{\text{res}}^{JP}(E_0))$ . Then  $\text{Tr } \mathbf{Q}_{\text{res}}^{JP}(E)$  was evaluated at two additional points,  $E_k = E_0 + k\Gamma_0/2$  for  $k = -1, 1$ , and these three points were used to fit the function  $\text{Tr } \mathbf{Q}_{\text{res}}^{JP}(E)$  (or  $\text{Tr } \mathbf{Q}^{JP}(E)$ ) to the following formula:

$$\text{Tr } \mathbf{Q}_{\text{res}}^{JP}(E) = \hbar \frac{\Gamma + 2r(E - E^{\text{res}})}{(E - E^{\text{res}})^2 + \Gamma^2/4} + C. \quad (17)$$

The parameters  $E^{\text{res}}$  and  $\Gamma$  obtained from the fit were considered to be the “true” energy and width of the state,  $E_{\bar{\nu}\bar{J}n\bar{I}J}$  and  $\Gamma_{\bar{\nu}\bar{J}n\bar{I}J}$ , respectively. The performance of the procedure in some representative cases of the Feshbach and shape resonances investigated in this work is demonstrated in Table I. The shifts  $E^{\text{res}} - E_0$  due to the asymmetry of the profiles were usually negligible. The changes of the  $\Gamma_0$ -estimates of the widths due to the background  $C$  of the profiles in  $\text{Tr } \mathbf{Q}^{JP}(E)$  were sometimes of the order of 5%. The consistency of the  $E^{\text{res}}$  and  $\Gamma$  parameters obtained from the analysis of both functions in the case of Feshbach resonances is believed to prove the reliability of this procedure.

## V. NUMERICAL RESULTS AND DISCUSSION

All bound states and 149 metastable (100 predissociating + 49 tunneling) states of the Ar–HD complex associated with 5 Ar+HD( $\bar{\nu}, \bar{J}$ ) dissociation thresholds,  $\bar{\nu}=0, \bar{J}=0, 1$  and  $\bar{\nu}=1, \bar{J}=0-2$ , were determined in this work from both

TABLE II. Bound and predissociating states of Ar–HD determined in this work.

Character of state	Assignment					No. of states	Threshold $\varepsilon_{\bar{v}\bar{j}}^a$
	$p$	$\bar{v}$	$\bar{j}$	$\bar{l}$	$n$		
Bound	(+) 0	0	0–7	0	8	0	
			0–2	1	3		
	(–) 0	1	1–7	0	7	89.228	
			1–2	1	2		
Predissociating: Vibrationally	(+) 1	0	0–7	0	8	3632.161	
			0–3	1	4		
	(–) 1	1	1–7	0	7	3717.533	
			1–3 <sup>b</sup>	1	3		
Rotationally	(+) 0	1	0–7	0	15	89.228	
	(+) 1	1	0–7	0	15	3717.533	
	(±) 1	2	0–7	0	34	3887.680	
			0–3	1	14		

<sup>a</sup>Theoretical values (in  $\text{cm}^{-1}$ ) from Ref. 75.

<sup>b</sup>The state with  $\bar{l}=3$  lies above the  $\varepsilon_{11}$ -threshold when determined from the SAPT potential.

the *ab initio* SAPT and the empirical XC(fit) potentials. A summary of the computed bound and predissociating states is given in Table II. It should be noted that in addition to the 11 bound states of  $p=1$  parity (*e* levels<sup>77</sup>), found also in the previous studies, there are 9 states of  $p=-1$  parity (*f* levels) associated with the ( $\bar{v}=0, \bar{j}=1$ ) threshold. The calculated energies and widths of all states, except for those associated with the ( $\bar{v}=1, \bar{j}=2$ ) threshold, are listed in Table III. The energies of a number of states not listed in Table III can be extracted from Tables V, VIII, and IIIa, and the widths are given in Tables VI and VIII. The widths listed in the fourth column of Table IIIb seem worth noting since they provide the first theoretical estimation of the vibrational predissociation in the Ar–HD complex. It turns out that this decay mechanism is as much as seven orders of magnitude slower than the rotational predissociation in the same complex but more than two order of magnitude faster than the vibrational predissociation in the Ar–H<sub>2</sub> complex, when estimated from the same (SAPT) potential.

In Tables IV–VI a comparison with experiment is made of individual results calculated for (A) the transition energies  $\Delta E$  in the  $Q_1(0)$  band, (a) the  $n'=0 \leftarrow n''=0$  transitions and (b) the transitions that involve an excited van der Waals stretch; (B) the  $\Delta E$  energies of the *N* and *T* transitions in the  $S_1(0)$  band; (C) the widths  $\Gamma$  of the lines corresponding to these transitions. In Table VII a summary of this comparison is presented in terms of relative (to the experimental uncertainties) root mean square deviations defined as

$$\bar{\delta}_r Y := \left[ \frac{1}{N_d} \sum_{i=1}^{N_d} (Y_i^{\text{cal}} - Y_i^{\text{exp}})^2 / u_i^2 \right]^{1/2}, \quad (18)$$

where  $Y_i^{\text{cal}}$  and  $Y_i^{\text{exp}}$  stand for the calculated and experimental values of  $\Delta E$  or  $\Gamma$ , respectively,  $u_i$  is the uncertainty of  $Y_i^{\text{exp}}$ , and  $N_d$  is the number of data in a given set, (A), (a), (b), (B), (C) or (c). In the latter set, the width of the *T*(7) line

is omitted with the conjecture that there are more transitions contributing to the experimental value of this width; see Figs. 3–4 and Table VIII.

As far as the XC potential is concerned, Table VII extends Table V of Ref. 14 providing further information on the ability of this potential to reproduce the experimental data not used in the fit. The deviations  $\bar{\delta}_r \Delta E < 1$  shown for the sets (a) and (B) of the transition energies mean that the corresponding (average) absolute deviations  $\bar{\delta} := \bar{u} \bar{\delta}_r$  are smaller than the average experimental uncertainty  $\bar{u}$  of these energies, i.e.,  $\bar{\delta} < 0.006 \text{ cm}^{-1}$ . Thereby, the high quality of the XC(fit) potential in the van der Waals well region is confirmed. The larger deviation for the set (b) may be a sign of a slight worsening of the fit in the upper parts of the potential well. The deviations  $\bar{\delta}_r \Gamma > 2.5$  and  $\bar{\delta} \Gamma > 0.15 \text{ cm}^{-1}$  for the sets (C) and (c) of the linewidths indicate, however, that the XC potential deteriorates significantly in the wall region, especially in the part just above the dissociation asymptote (as this is the part to which the widths are most sensitive, cf. Ref. 13).

Concerning the SAPT potential, the general conclusions drawn from Tables IV–VII are as follows. The potential reproduces the experimental transition energies in both the  $Q_1(0)$  and  $S_1(0)$  bands and the linewidths in the latter band roughly with the same absolute deviations  $\bar{\delta}$ , of the order of  $0.1 \text{ cm}^{-1}$ . These deviations are comparable with the experimental uncertainties of the data for the  $S_1(0)$  band (as the  $\bar{\delta}_r$ 's for  $\Delta E$  and  $\Gamma$  are 1.2 and 1.31, respectively) and exceed  $\approx 10$  times the average uncertainty  $\bar{u} = 0.009 \text{ cm}^{-1}$  of the measured energies in the  $Q_1(0)$  band. Thus, the *ab initio* SAPT potential, though evidently needing improvement, appears to be more uniform in accuracy along both the wall and well regions, and is more accurate than the empirical potential in the wall region. The latter fact is the most encouraging as there seem to be major difficulties in modelling the repulsive walls of the empirical potentials.

On the basis of the information presented in Tables III and II reliable theoretical predictions can be made for the transition energies in the  $Q_1(1)$  band. The energies predicted from the XC potential for 130 transitions in this band are presented in Fig. 1 together with all the energies measured in the  $Q_1(0)$  band and 8 additionally calculated for the  $n=0 \leftarrow -1$  and  $n=1 \leftarrow 0$  transitions. Transitions belonging to different subbranches of the *P* and *R* branches of the  $Q_1(1)$  band are represented in Fig. 1 by lines of different lengths. The lengths are chosen to show schematically relations between the subbranches with respect to the expected average widths of the peaks (lines) in the spectrum. Obviously, the sharpest peaks are expected for the  $R_+(\bar{l}, \bar{l})$  and the  $P_-(\bar{l}, \bar{l})$  transitions (the longest lines in the upper panel of the figure) as they involve bound and vibrationally predissociating states only. On the same ground one can expect that the second sharpest should be the peaks of the  $P_0(\bar{l}, \bar{l}-1)$  and  $R_0(\bar{l}, \bar{l})$  transitions. They involve rotationally predissociating states on one end, the states ( $\bar{v}=0, \bar{j}=1, n=0, \bar{l}, J=\bar{l}-1$ ) and ( $\bar{v}=1, \bar{j}=1, n=0, \bar{l}+1, \bar{l}$ ), respectively, but the widths of these states are the smallest among the rotationally predisso-

TABLE III. (a) Energies<sup>a</sup> and widths (both in cm<sup>-1</sup>) of the Ar-HD states calculated from the SAPT and XC potentials. All bound and some tunneling states.<sup>b</sup> (b) Energies<sup>a</sup> and widths<sup>c</sup> of the ( $\bar{\nu}=1; \bar{J}=0, 1; \bar{I}; n; J\bar{I}$ ) states of Ar-HD. (c) Energies and widths of the ( $\bar{\nu}=0, 1; \bar{J}=1; n=0; \bar{I}; J=\bar{I}\pm 1$ ) states of Ar-HD calculated from the XC potential.

(a)		$\bar{\nu}=0 \bar{J}=0$		$\bar{\nu}=0 \bar{J}=1$		
$n$	$\bar{I}=\bar{J}$	SAPT	XC	SAPT	XC	
0	0	-25.605	-25.603			
	1	-24.804	-24.807	-23.995	-24.141	
	2	-23.208	-23.222	-22.397	-22.553	
	3	-20.828	-20.857	-20.015	-20.185	
	4	-17.680	-17.730	-16.866	-17.055	
	5	-13.790	-13.867	-12.976	-13.188	
	6	-9.194	-9.302	-8.382	-8.621	
	7	-3.942	-4.087	-3.140	-3.410	
	8	1.882	1.697	2.659	2.361	
			0.85(-5)	0.39(-5)	0.14(-3)	0.57(-4)
	9	8.095	7.870	8.806	8.481	
			0.74(-1)	0.65(-1)	0.13	0.11
10		14.549	14.272	15.219	14.849	
		0.88	0.83	1.15	1.06	
	11	21.473	21.132	22.157	21.717	
		2.91	2.83	3.41	3.26	
12		29.062	28.630			
		6.16	6.05			
	1	-2.149	-2.258			
	1	-1.732	-1.838	-1.523	-1.662	
	2	-0.931	-1.030	-0.746	-0.872	
	3	0.149	0.072			
		0.35(-2)	0.31(-3)			

(b)		$\bar{\nu}=1 \bar{J}=0$			$\bar{\nu}=1 \bar{J}=1$	
$n$	$\bar{I}$	SAPT		XC	$E$	
		$E$	$\Gamma$	$E$	SAPT	XC
0	0	-26.416	0.41(-7)	-26.515		
	1	-25.623	0.41(-7)	-25.724	-24.676	-25.022
	2	-24.042	0.39(-7)	-24.147	-23.095	-23.441
	3	-21.685	0.37(-7)	-21.795	-20.735	-21.084
	4	-18.566	0.34(-7)	-18.685	-17.615	-17.966
	5	-14.709	0.30(-7)	-14.839	-13.758	-14.113
	6	-10.148	0.26(-7)	-10.292	-9.199	-9.562
	7	-4.929	0.22(-7)	-5.090	-3.989	-4.355
	8	0.875	0.34(-7)	0.692	1.784	1.420
			0.16(-7)	0.25(-8)	0.58(-5)	0.95(-6)
9		7.113		6.908	7.957	7.595
		0.29(-1)		0.25(-1)	0.69(-1)	0.51(-1)
	1	-2.401		-2.571		
1	1	-1.977		-2.141	-1.716	-1.933
	2	-1.158		-1.308	-0.924	-1.119
	3	-0.027		-0.151		-0.001

(c)		$\bar{\nu}=0 \bar{J}=1$				$\bar{\nu}=1 \bar{J}=1$			
$\bar{I}$	$J=\bar{I}-1$	$J=\bar{I}+1$		$J=\bar{I}-1$		$J=\bar{I}+1$			
		$E$	$\Gamma$	$E$	$\Gamma$	$E$	$\Gamma$		
0			-25.70	1.20			-26.59	1.49	
1	-25.75	1.73	-24.93	1.05	-26.66	2.09	-25.82	1.29	
2	-23.42	0.52	-23.37	0.98	-24.35	0.60	-24.28	1.20	
3	-21.04	0.60	-21.04	0.92	-21.97	0.72	-21.96	1.12	
4	-17.91	0.60	-17.94	0.85	-18.85	0.72	-18.89	1.05	
5	-14.05	0.57	-14.10	0.78	-15.01	0.69	-15.08	0.96	
6	-9.49	0.52	-9.56	0.70	-10.48	0.63	-10.56	0.86	
7	-4.29	0.46	-4.37	0.60	-5.29	0.55	-5.39	0.75	
8	1.49	0.38	1.40	0.50	0.48	0.47	0.37	0.63	
9	7.67	0.34	7.58	0.42	6.70	0.38	6.58	0.50	
10	14.05	0.96	13.97	0.99	13.11	0.75	13.01	0.82	

<sup>a</sup>Energies are relative to the respective  $\varepsilon_{\bar{\nu}\bar{J}}$ -energies of HD listed in Table II.

<sup>b</sup>Widths of the tunneling states are listed below the energies.

<sup>c</sup>The widths of the tunneling state are shown as in (a); the widths due to the vibrational predissociation, calculated from the SAPT potential only, are shown in a separate column.

TABLE IV. Transition frequencies  $\Delta E$  (in  $\text{cm}^{-1}$ ) in the  $Q_1(0)$  band of the Ar–HD near-infrared spectrum. Comparison of the results calculated from the SAPT and XC potentials with the experiment (Ref. 9). The absolute error between theory and experiment is defined by  $\delta = \Delta E(\text{cals.}) - \Delta E(\text{expt.})$ .

Transition	$n'' \rightarrow n'$	SAPT		XC	
		$\Delta E$	$\delta$	$\Delta E$	$\delta$
<i>R</i> (2)	1 0	3611.407	-0.007	3611.396	-0.018
<i>R</i> (3)		3613.446	-0.002	3613.405	-0.061
<i>P</i> (9)	0 0	3624.941	-0.056	3624.983	-0.014
<i>P</i> (8)		3625.351	-0.024	3625.374	-0.001
<i>P</i> (7)		3625.955	-0.003	3625.956	-0.002
<i>P</i> (6)		3626.646	0.024	3626.624	0.002
<i>P</i> (5)		3627.386	0.048	3627.343	0.005
<i>P</i> (4)		3628.156	0.066	3628.096	0.006
<i>P</i> (3)		3628.946	0.079	3628.871	0.004
<i>P</i> (2)		3629.747	0.096	3629.659	0.008
<i>P</i> (1)		3630.550	0.092	3630.454	-0.004
<i>R</i> (0)		3632.143	0.102	3632.040	-0.001
<i>R</i> (1)		3632.923	0.106	3632.821	0.004
<i>R</i> (2)		3633.685	0.096	3633.587	0.002
<i>R</i> (3)		3634.423	0.089	3634.333	-0.001
<i>R</i> (4)		3635.132	0.082	3635.052	0.002
<i>R</i> (5)		3635.804	0.064	3635.736	-0.004
<i>R</i> (6)		3636.426	0.051	3636.372	-0.003
<i>R</i> (7)		3636.978	0.031	3636.940	-0.007
<i>R</i> (8)		3637.393	0.013	3637.372	-0.008
<i>P</i> (4)	0 1	3649.814	0.102	3649.741	0.029
<i>P</i> (3)		3651.831	0.137	3651.710	0.016
<i>P</i> (2)		3653.392	0.170	3653.242	0.020
<i>R</i> (2)		3655.342	0.120	3655.232	0.010

ciating states with  $\bar{J}=1$ , cf. Table IIIc. Other transitions in the  $Q_1(1)$  band originate and/or terminate on the rotationally predissociating states which are characterized by widths even larger than those measured in the  $S_1(0)$  band, and evidently larger than those calculated for the *R* and *P* transitions in this

TABLE V. Transition frequencies  $\Delta E$  (in  $\text{cm}^{-1}$ ) in the *N* and *T* branches of the  $S_1(0)$  band<sup>a</sup> of the Ar–HD near-infrared spectrum. Comparison of the results calculated from the SAPT and XC potentials with the experiment (Ref. 7). The absolute error between theory and experiment is defined by  $\delta = \Delta E(\text{calc.}) - \Delta E(\text{expt.})$ .

Transition $n' = n'' = 0$	SAPT		XC	
	$\Delta E$	$\delta$	$\Delta E$	$\delta$
<i>N</i> (10)	3867.93		3868.15	
<i>N</i> (9)	3869.23	-0.05	3869.41	0.13
<i>N</i> (8)	3870.94	-0.19	3871.09	-0.04
<i>N</i> (7)	3872.96	-0.13	3873.08	-0.01
<i>N</i> (6)	3875.15	-0.11	3875.24	-0.02
<i>N</i> (5)	3877.45	-0.06	3877.50	-0.01
<i>N</i> (4)	3879.82		3879.85	
<i>N</i> (3)	3882.28		3882.27	
<i>T</i> (0)	3891.21		3891.29	
<i>T</i> (1)	3893.58		3893.62	
<i>T</i> (2)	3895.84	-0.05	3895.86	-0.03
<i>T</i> (3)	3898.00	-0.04	3898.01	-0.03
<i>T</i> (4)	3900.04	-0.04	3900.04	-0.04
<i>T</i> (5)	3901.91	0.02	3901.91	0.02
<i>T</i> (6)	3903.54	0.01	3903.54	0.01
<i>T</i> (7)	3904.74	0.01	3904.72	-0.01

<sup>a</sup>The energy of the  $S_1(0)$  transition in HD is  $\varepsilon_{12} = 3887.680 \text{ cm}^{-1}$ .

TABLE VI. Widths  $\Gamma$  (in  $\text{cm}^{-1}$ ) of the ( $\bar{\nu}=1, \bar{J}=2, \bar{I}, n=0, J=\bar{I} \pm 2$ ) states of Ar–HD. Comparison of the theoretical results calculated from the SAPT and XC potentials with the experimental line widths in the  $S_1(0)$  band.

$\bar{I}$	$J$	Calculated		Expt. <sup>a</sup>
		SAPT	XC	
7	9	0.555	0.477	
6	8	0.625	0.536	0.59(7) <sup>b</sup>
5	7	0.682	0.583	0.73(7)
4	6	0.726	0.619	0.74(7)
3	5	0.757	0.641	0.78(8)
2	4	0.774	0.650	0.87(10)
1	3	0.773	0.642	
0	2	0.769	0.617	
3	1	0.910	0.805	
4	2	0.764	0.676	
5	3	0.668	0.586	0.84(10)
6	4	0.581	0.505	0.68(6)
7	5	0.494	0.426	0.56(4)
8	6	0.413	0.347	0.47(3)
9	7	0.323	0.274	0.38(3)
10	8	0.700	0.658	1.33(19)

<sup>a</sup>Reference 9.

<sup>b</sup>The experimental uncertainties are given in parentheses.

band, cf. Table VIII. The overall increase of the widths of the ( $\bar{\nu}=1, \bar{J}=1, \bar{I}, J=\bar{I} \pm 1$ ) states over the widths of the ( $\bar{\nu}=1, \bar{J}=2, \bar{I}, J=\bar{I} \pm 2$ ) states can be rationalized by the positions of these states on the energy scale relative to the thresholds of the nearby continuum states. Whereas the former states lie from about  $63.5 \text{ cm}^{-1}$  to  $103.3 \text{ cm}^{-1}$  above the  $\varepsilon_{1,0}$  threshold the latter are in the range from  $143 \text{ cm}^{-1}$  to  $184 \text{ cm}^{-1}$  above their respective threshold  $\varepsilon_{1,1}$ . Consequently, there should be a larger overlap of the functions of the discrete and continuum states contributing to the widths in the former cases.

The predictions made here for the  $Q_1(1)$  band, and especially the picture of the positions of lines relative to the  $Q_1(0)$  band, are hoped to be helpful in assigning more features in the observed contour of these overlapping bands. For example, the small peak appearing between the *R*(6) and

TABLE VII. Relative root mean square deviations from the experiment of the transitions frequencies and line widths in the near-infrared spectrum of Ar–HD calculated from the SAPT and XC potentials.

$Y$	$N_d$	$\bar{u}^a$	$\bar{\delta}_r Y$	
			SAPT	XC
<i>Q</i> <sub>1</sub> (0) band:				
(A) energies of all transitions measured	24	0.009	11.24	1.12
(a) energies of $n=0 \leftarrow 0$ transitions	18	0.006	12.33	0.86
(b) energies of transitions with $n'=1$ or $n''=1$	6	0.018	7.01	1.68
<i>S</i> <sub>1</sub> (0) band:				
(B) energies of <i>N</i> and <i>T</i> transitions <sup>b</sup>	11	0.076	1.20	0.72
(C) widths of <i>N</i> and <i>T</i> lines	11	0.076	1.61	2.76
(c) the set (C) with the <i>T</i> (7) line excluded	10	0.065	1.32	2.67

<sup>a</sup>Average experimental uncertainty (in  $\text{cm}^{-1}$ ).

<sup>b</sup>The experimental uncertainties of these energies were set equal to the uncertainties of the corresponding widths quoted in Table VI.

TABLE VIII. Frequencies  $\Delta E$ , widths of the upper states (both in  $\text{cm}^{-1}$ ), and intensities (in arbitrary units) of the transitions<sup>a</sup> in the  $S_1(0)$  band of the Ar–HD near-infrared spectrum calculated from the XC potential.

Transition <sup>b</sup>	$\Delta E$	Intensity	$\Gamma$	Transition <sup>b</sup>	$\Delta E$	Intensity	$\Gamma$
$N(11)$	3867.100	0.91(-5)	0.40	$R_+(1)$	3888.888	0.12(-4)	0.27
$N(10)$	3868.147	0.21(-4)	0.48	$R_-(2)$	3888.913	0.90(-5)	0.80
$N(9)$	3869.406	0.51(-4)	0.54	$R_0(2)$	3889.293	0.23(-4)	0.31
$N(8)$	3871.089	0.59(-4)	0.58	$R_-(3)$	3889.668	0.97(-5)	0.68
$N(7)$	3873.083	0.59(-4)	0.62	$R_+(2)$	3889.705	0.22(-4)	0.26
$N(6)$	3875.240	0.56(-4)	0.64	$T(0;1,1)$	3889.774	0.47(-5)	0.19
$N(5)$	3877.504	0.51(-4)	0.65	$R_0(3)$	3890.100	0.33(-4)	0.26
$N(4)$	3879.846	0.43(-4)	0.64	$R_-(4)$	3890.369	0.11(-4)	0.59
$P_+(9)$	3880.274	0.65(-5)	0.40	$R_+(3)$	3890.454	0.33(-4)	0.25
$P_-(11)$	3880.357	0.39(-5)	0.78	$T_+(1;1,1)$	3890.592	0.27(-5)	0.38
$P_0(10)$	3880.686	0.66(-5)	0.15	$R_0(4)$	3890.841	0.43(-4)	0.22
$P_+(8)$	3880.720	0.72(-5)	0.48	$R_-(5)$	3891.019	0.12(-4)	0.50
$P_-(10)$	3880.833	0.95(-5)	0.15	$R_+(4)$	3891.178	0.44(-4)	0.23
$P_0(9)$	3880.925	0.33(-4)	0.15	$T(0)$	3891.294	0.20(-4)	0.80
$P_-(9)$	3881.069	0.46(-4)	0.14	$R_0(5)$	3891.531	0.53(-4)	0.18
$P_0(8)$	3881.351	0.47(-4)	0.17	$R_-(6)$	3891.612	0.13(-4)	0.43
$P_+(7)$	3881.363	0.71(-5)	0.54	$R_+(5)$	3891.856	0.54(-4)	0.20
$P_-(8)$	3881.481	0.64(-4)	0.17	$R_-(7)$	3892.133	0.14(-4)	0.35
$P_0(7)$	3881.964	0.45(-4)	0.19	$R_0(6)$	3892.164	0.64(-4)	0.15
$P_-(7)$	3882.076	0.61(-4)	0.20	$R_+(6)$	3892.480	0.64(-4)	0.17
$P_+(6)$	3882.088	0.66(-5)	0.58	$R_-(8)$	3892.542	0.14(-4)	0.27
$N(3)$	3882.273	0.34(-4)	0.62	$R_0(7)$	3892.718	0.76(-4)	0.12
$P_0(6)$	3882.661	0.42(-4)	0.20	$R_-(9)$	3892.768	0.51(-5)	0.66
$P_-(6)$	3882.750	0.57(-4)	0.23	$R_+(7)$	3893.026	0.73(-4)	0.14
$P_+(5)$	3882.863	0.60(-5)	0.62	$R_0(8)$	3893.124	0.65(-4)	0.12
$P_0(5)$	3883.411	0.38(-4)	0.21	$R_0(9)$	3893.356	0.94(-5)	0.69
$P_-(5)$	3883.464	0.52(-4)	0.25	$R_+(8)$	3893.408	0.60(-4)	0.15
$P_+(4)$	3883.668	0.51(-5)	0.64	$T(1)$	3893.618	0.38(-4)	0.68
$P_0(4)$	3884.198	0.33(-4)	0.20	$R_+(9)$	3893.619	0.10(-4)	0.78
$P_-(4)$	3884.213	0.45(-4)	0.26	$R_0(10)$	3893.776	0.29(-5)	2.46
$P_+(3)$	3884.494	0.40(-5)	0.65	$R_+(10)$	3894.039	0.36(-5)	2.64
$P_-(3)$	3884.938	0.36(-4)	0.27	$T(2)$	3895.861	0.57(-4)	0.59
$P_0(3)$	3885.020	0.27(-4)	0.19	$N(6;0,1)$	3896.866	0.71(-5)	0.14
$P_-(2)$	3885.091	0.23(-4)	0.79	$T(3)$	3898.009	0.77(-4)	0.50
$P_0(2)$	3885.888	0.20(-4)	0.15	$T(4)$	3900.049	0.98(-4)	0.43
$P_-(3;1,1)$	3886.451	0.60(-5)	0.01	$N(5;0,1)$	3900.305	0.66(-5)	0.19
$P_0(3;1,1)$	3886.484	0.54(-5)	0.05	$T(5)$	3901.913	0.12(-3)	0.35
$P_-(2;1,1)$	3886.602	0.45(-5)	0.26	$P_+(5;0,1)$	3902.666	0.58(-5)	0.39
$P_0(2;1,1)$	3886.794	0.48(-5)	0.04	$N(4;0,1)$	3903.366	0.60(-5)	0.20
$R_-(1)$	3888.103	0.11(-4)	1.13	$T(6)$	3903.541	0.14(-3)	0.27
$R_0(1;1,1)$	3888.242	0.36(-5)	0.14	$T(7)$	3904.725	0.49(-4)	0.66
$R_0(1)$	3888.310	0.14(-4)	0.48	$P_-(4;0,1)$	3905.386	0.82(-5)	0.07
$R_0(2;1,1)$	3888.611	0.62(-5)	0.08	$P_0(4;0,1)$	3905.393	0.39(-5)	0.04
$R_+(2;1,1)$	3888.686	0.35(-5)	0.07	$T_+(8)$	3905.720	0.13(-4)	2.20

<sup>a</sup>Listed are all the transitions with frequencies in the range  $3865\text{--}3906\text{ cm}^{-1}$  whose intensities are not smaller than 0.02 of the largest (in this range) intensity of the  $T(6)$  transition.

<sup>b</sup>See Sec. III for an explanation of the notation used.

$R(7)$  lines in the contour of  $Q_1(0)$  shown in Fig. 7 of Ref. 7 seems to be a trace of the  $T(2,3)$  transition of energy  $\Delta E = 3636.67\text{ cm}^{-1}$  in  $Q_1(1)$ .

In Fig. 2 further information is given on how the widths of states predicted from the XC potential, listed in Tables IIIc and VIII, compare with the widths resulting from the SAPT potential. They are shown to be generally smaller than the SAPT widths which points to smaller strength  $|\bar{V}_1(R,r)|$  of the first-order anisotropy of the XC potential for  $R$  in the part of the repulsive wall region extending from about 2.9 Å to 3.2 Å. The largest absolute deviations between the XC and SAPT results occur for the largest widths, revealed by the  $(\bar{v}=1, \bar{J}=1, \bar{I}, J=\bar{I}+1)$  states. In terms of average relative deviations defined as

$$\text{rel. dev. } \Gamma := \frac{1}{N_d} \sum_i^{N_d} |1 - \Gamma_i^{\text{XC}} / \Gamma_i^{\text{SAPT}}| 100\%, \quad (19)$$

the two sets of results for the three  $(\bar{v}, \bar{J})$  cases shown in Fig. 2, (0,1), (1,1), and (1,2), differ by 7%, 12%, and 18%, respectively. The relative deviation of the widths listed in Table VI is 14%. The deviations in the  $\bar{v}=1$  cases being so much larger than in the  $\bar{v}=0$  case indicate that important differences occur between the XC and SAPT potentials for Ar–HD with respect to the  $r$ -dependence of the  $\bar{V}_1(R,r)$  strength function for  $R$  corresponding to the repulsive wall region. This indication is indeed consistent with what is shown in Fig. 3 of Ref. 14 concerning the radial strength

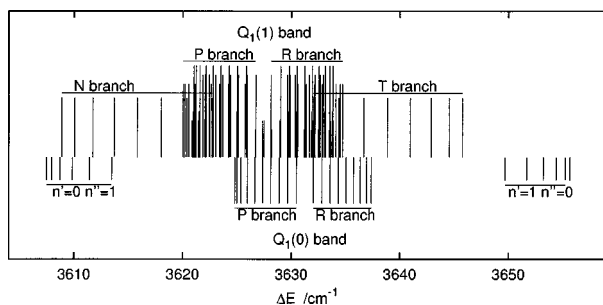


FIG. 1. Near-infrared transitions in the  $Q_1(1)$  and  $Q_1(0)$  bands of the Ar-HD spectrum. The six subbranches of the  $P$  and  $R$  transitions in the  $Q_1(1)$  band are described by lines with length decreasing in the following order:  $P_-(\bar{T}, \bar{T}), R_+(\bar{T}, \bar{T})$ ;  $P_0(\bar{T}, \bar{T}-1), R_0(\bar{T}, \bar{T})$ ;  $P_0(\bar{T}, \bar{T}), R_0(\bar{T}, \bar{T}+1)$ ;  $P_-(\bar{T}, \bar{T}-1), R_+(\bar{T}, \bar{T}-1)$ ;  $P_+(\bar{T}, \bar{T}-1), R_-(\bar{T}, \bar{T}+1)$ ;  $P_-(\bar{T}, \bar{T}+1), R_+(\bar{T}, \bar{T}+1)$ .

functions  $V_{0,0}(R)$  and  $V_{0,1}(R)$  of these potentials for Ar-H<sub>2</sub> [cf. Eq. (15)]; note also that for Ar-HD the derivatives of these functions contribute most essentially to the respective functions  $\bar{V}_{1,0}(R)$  and  $\bar{V}_{1,1}(R)$  [Eq. (15) of Ref. 42].

In Figs. 3–5 and in Table VIII results of the intensity calculations for the transitions in the  $S_1(0)$  band are shown. Obviously, all the intensities presented should be understood as relative intensities only. To mark that, the term “arbitrary units” is put in the labels of the ordinate axes in the figures and in the caption to the table. Actually, the numbers listed as intensities in Table VIII are given in Å<sup>2</sup> and represent maxima in the thermally averaged partial photodissociation or phototransition cross sections,  $\sigma^{\max}(J_i; p_i)$ , i.e., they are values of the individual terms in the sums (7) or (6) at photon energies equal to energy differences  $\Delta E$  between the final and initial states of the transitions indicated. The Boltzmann factor in the unnormalized form (with  $Z = 1$ , cf. Sec. II) was used for the thermal averaging (at  $T = 77$  K) and the

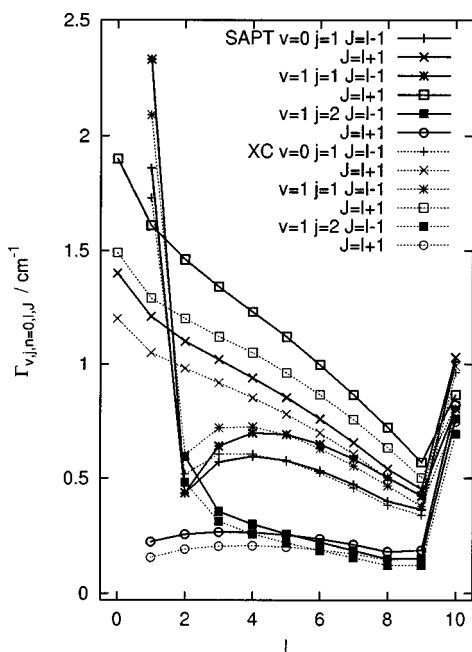


FIG. 2. Widths of the rotationally predissociating states of Ar-HD.

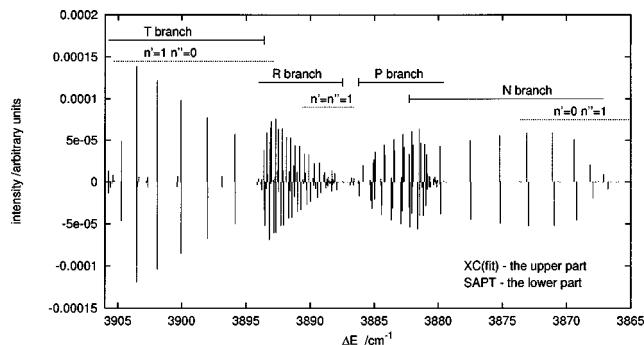


FIG. 3. Near-infrared transitions in the  $S_1(0)$  band of the Ar-HD spectrum.

zero of the energy scale was shifted in this factor from the lowest dissociation threshold of the complex to the lowest bound state level.

Figure 3 gives a summary of the information generated for 111 individual transitions in the  $S_1(0)$  band; the transition energies  $\Delta E$  and the intensities  $\sigma^{\max}$  are presented, and a comparison is made between the results calculated from the XC and SAPT potentials. The largest intensities are seen in the  $T$  branch.  $T(6)$ —the most intense transition in the entire band—is approximately twice as intense as the transitions in the  $N$  branch. Of the groups of transitions involving excited van der Waals stretching states the largest intensities, reaching the level of a few percent of the  $T(6)$  intensity, are seen in the  $n = 1 \leftarrow 0$  group. Two of the most intense transitions of this group,  $P_-(4)$  and  $P_0(4)$ , occur in the vicinity of the  $T(7)$  line, at a distance close to its calculated width (cf. Table VIII). It seems likely that all these transitions might have been observed in the experiment as one broad line. This would explain the failure of all calculations done so far (see Table X of Ref. 9 and Table VI of this work) in reproducing the experimental width of the  $T(7)$  line. Concerning the comparison of the SAPT and XC results, Fig. 3 and also Fig. 5(a) and 5(b) reveal that such a good agreement of the transition energies, as shown in Table V for the  $T$  and  $N$  branches, does not hold for the  $R$  and  $P$  branches. Like in the  $Q_1(0)$  band, cf. Table IV, the SAPT and XC results differ mostly for the transitions labeled by low  $\bar{T}$ 's, in the central part of the band. In the  $S_1(0)$  band, however, the differences

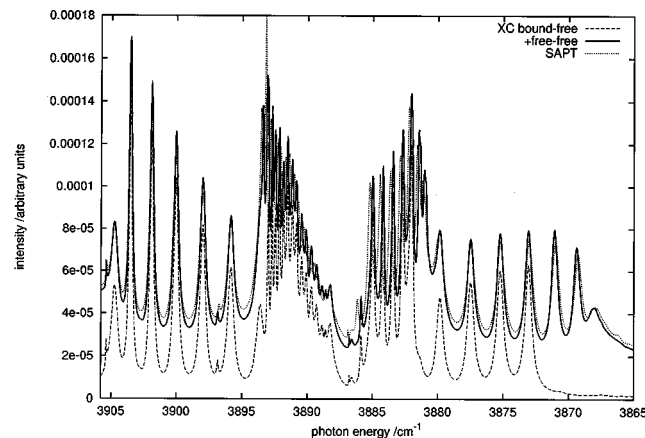


FIG. 4. Near-infrared absorption spectrum of Ar-HD in the  $S_1(0)$  band.

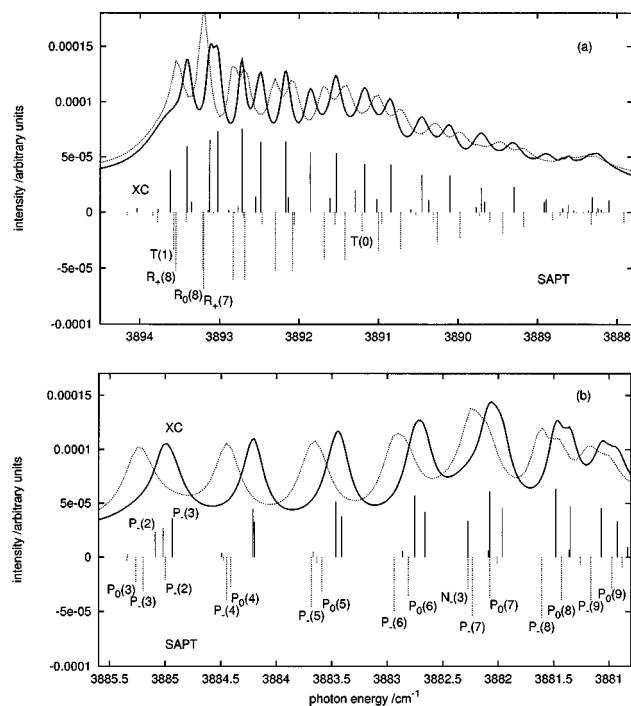


FIG. 5. Near-infrared absorption spectrum of Ar-HD. (a)  $R$  transition and (b)  $P$  transition regions of the  $S_1(0)$  band.

are more than two times larger. This may be understood as an effect of accumulated inaccuracies in the isotropic and anisotropic terms of the SAPT potential in the well region. Some differences can also be noticed in Fig. 3 between the SAPT and XC results for the maximal intensities of transitions. Since the same model of the induced dipole was used in both cases, the differences should be connected with the different widths of lines resulting from the two potentials. Indeed, when the integrated intensities of lines, proportional to  $\sigma^{\max}\Gamma$ , are compared, the XC and SAPT results agree much better, within a few percent for the  $T$  lines.

The results of simulations of the shape of the  $S_1(0)$  band carried out in this work are presented in Figs. 4 and 5. Three contours are shown in Fig. 4. The one drawn with a broken line has been obtained by evaluating only the  $\sigma_{F\leftarrow B}$  term in Eq. (2) and therefore it represents essentially the same dynamical approach as employed in the previous line shape study of this band.<sup>28</sup> Compared to the result of this study, cf. Fig. 1 of Ref. 28, the contour does not show much difference. In particular, the relative intensities of lines in the  $N$  branch remain the same. Comparison of the “bound-free contour” with the two other contours shown in Fig. 4 exhibits, however, quite pronounced changes due to the free-free type transitions included in the  $\sigma_{F\leftarrow F}^{\text{res}}$  term of Eq. (2). The improvement of the picture of relative intensities in the  $N$  and  $P$  branches achieved over the previous simulation is remarkable, the more so as the same model of the induced dipole was adopted.

The contour drawn with the full line is considered as the best result of the present simulations. Since it is obtained from the XC potential it is certainly reliable with respect to the position of the lines. With respect to the widths and heights of the lines in the  $N$  and  $T$  transition regions, how-

ever, the XC contour is slightly inferior to that generated from the SAPT potential.

For a confrontation with experiment of the shape of the  $S_1(0)$  band simulated from the XC and SAPT potentials, the contours drawn in Fig. 4 with the full and dotted lines, respectively, should be compared with the contour shown in the lower panel of Fig. 11 of Ref. 9. The overall agreement of the theoretical and experimental contours is very good. The only major discrepancy is the excessive peak in the SAPT contour appearing at the edge of the  $R$  transition region. In the expanded view of this region, given in Fig. 5(a), the peak is shown to arise from too strong an overlapping of two intense lines,  $R_0(8)$  and  $R_+(7)$ , and therefore it certainly should be attributed to an inaccuracy of the SAPT potential in the well region. The simulated contours, especially the XC contour, are of such a quality that an assignment of the individual peaks in the middle part of the observed band can be attempted on their basis. This is done for the  $P$  transition region in Fig. 5(b) and partly for the  $R$  transition region, in Fig. 5(a). Complete information necessary to assign all peaks discernible in this band can be found in Table VIII.

## ACKNOWLEDGMENTS

We are grateful to Professor G. H. F. Diercksen for the hospitality extended to us during our stay at the Max-Planck-Institut für Astrophysik in Garching where this work was started. We thank Professor B. Jeziorski for critical reading of the manuscript.

## APPENDIX: RADIAL COMPONENTS OF THE INDUCED-DIPOLE MOMENT FUNCTION FOR Ar-HD

The derivation of the radial components of the Ar-HD induced-dipole starts from the relation

$$\bar{d}_q(\mathbf{r}, \mathbf{R}) := d_q(\mathbf{r}, \bar{\mathbf{R}}) = \frac{4\pi}{\sqrt{3}} \sum_{L\Lambda} d_{L\Lambda}(r, \bar{R}) \mathcal{Y}_{L\Lambda}^{1q}(\hat{\mathbf{r}}, \hat{\bar{\mathbf{R}}}),$$

where  $\bar{\mathbf{R}} := \mathbf{R} + f\mathbf{r}$ , and proceeds in two steps. In the first step, it is shown that

$$\bar{d}_q(\mathbf{r}, \mathbf{R}) = \frac{4\pi}{\sqrt{3}} \sum_{l\lambda} a_{l\lambda}(r, R, \bar{R}) \mathcal{Y}_{l\lambda}^{1q}(\hat{\mathbf{r}}, \hat{\mathbf{R}}), \quad (\text{A1})$$

where

$$a_{l\lambda}(r, R, \bar{R}) = \sum_{L\Lambda} (fr/R)^{\Lambda-\lambda} (R/\bar{R})^{\Lambda} \underbrace{d_{L\Lambda}(r, \bar{R})}_{\beta_{L\Lambda;l\lambda}},$$

$$\begin{aligned} \beta_{L\Lambda;l\lambda} &= \left[ \frac{[L][\Lambda]}{[l][\lambda]} \right]^{1/2} C(L\Lambda - \lambda l, 000) \\ &\times \sum_{m\mu} \left[ \binom{\Lambda + q - m}{\Lambda - \lambda + \mu} \binom{\Lambda - q + m}{\Lambda - \lambda - \mu} \right]^{1/2} \\ &\times C(L\Lambda 1, m q - m q) C(L\Lambda - \lambda l, m \mu m + \mu) \\ &\times C(l\lambda 1, m + \mu q - m - \mu q), \end{aligned}$$

and  $[L]:=L(L+1)$ . In the second step, the underbraced part of  $a_{l\lambda}$  is expanded in terms of Legendre polynomials,

$$(R/\bar{R})^\lambda d_{L\lambda}(r, \bar{R}) = \sum_K d_{L\lambda}^K(r, R) P_K(\cos(\hat{\mathbf{r}} \cdot \hat{\mathbf{R}})),$$

leading to the final expansion (16), and the following expression for the expansion coefficients:

$$\bar{d}_{L\lambda}^{\bar{K}}(r, R) = \sum_{L\lambda} \sum_{l\lambda} (fr/R)^{\lambda-l} \beta_{L\lambda;l\lambda} \sum_K \omega_{l\lambda;L\lambda}^K d_{L\lambda}^K(r, R), \quad (\text{A2})$$

where

$$\begin{aligned} \omega_{l\lambda;L\lambda}^K &= \left[ \frac{[l][\lambda]}{[L][\bar{\lambda}]} \right]^{1/2} C(Kl\bar{L}, 000) C(K\lambda\bar{\lambda}, 000) \\ &\times \sum_{m\mu} (-1)^\mu C(l\lambda 1, m\mu - m\mu) \\ &\times C(Kl\bar{L}, \mu m m + \mu) C(K\lambda\bar{\lambda}, -\mu\mu - m\mu - m - \mu) \\ &\times C(\bar{L}\bar{\lambda} 1, \mu + m\mu - m - \mu\mu). \end{aligned}$$

- <sup>1</sup> A. Kudian, H. L. Welsh, and A. Tanabe, *J. Chem. Phys.* **43**, 3397 (1965).
- <sup>2</sup> A. Kudian, H. L. Welsh, and A. Tanabe, *J. Chem. Phys.* **47**, 1553 (1967).
- <sup>3</sup> A. Kudian and H. L. Welsh, *Can. J. Phys.* **49**, 230 (1971).
- <sup>4</sup> A. R. W. McKellar and H. L. Welsh, *J. Chem. Phys.* **55**, 595 (1971).
- <sup>5</sup> A. R. W. McKellar and H. L. Welsh, *J. Chem. Phys.* **50**, 1458 (1972).
- <sup>6</sup> A. R. W. McKellar, *J. Chem. Phys.* **61**, 4636 (1974).
- <sup>7</sup> A. R. W. McKellar, *Faraday Discuss. Chem. Soc.* **73**, 89 (1982).
- <sup>8</sup> A. R. W. McKellar, in: *Structure and Dynamics of Weakly Bound Molecular Complexes*, NATO ASI Series, Series C, edited by A. Weber (Reidel, Dordrecht, 1987), Vol. 212, p. 141.
- <sup>9</sup> A. R. W. McKellar, *J. Chem. Phys.* **105**, 2628 (1996).
- <sup>10</sup> R. J. Le Roy and J. Van Kranendonk, *J. Chem. Phys.* **61**, 4750 (1974).
- <sup>11</sup> A. M. Dunker and R. G. Gordon, *J. Chem. Phys.* **68**, 700 (1978).
- <sup>12</sup> R. J. Le Roy and J. S. Carley, *Adv. Chem. Phys.* **42**, 353 (1980).
- <sup>13</sup> R. J. Le Roy and J. M. Hutson, *J. Chem. Phys.* **86**, 837 (1987).
- <sup>14</sup> C. Bissonnette, C. E. Chuaqui, K. G. Crowell, R. J. Le Roy, R. J. Wheatley, and W. J. Meath, *J. Chem. Phys.* **105**, 2639 (1996).
- <sup>15</sup> M. Waaijer, M. Jacobs, and J. Reuss, *Chem. Phys.* **63**, 247 (1981); **63**, 257 (1981).
- <sup>16</sup> U. Buck, *Faraday Discuss. Chem. Soc.* **73**, 187 (1982).
- <sup>17</sup> U. Buck, H. Meyer, and R. J. Le Roy, *J. Chem. Phys.* **80**, 5589 (1984).
- <sup>18</sup> R. L. Farrow, L. A. Rahn, G. O. Sitz, and G. J. Rosasco, *Phys. Rev. Lett.* **63**, 746 (1989).
- <sup>19</sup> J. Ph. Berger, R. Saint-Loup, H. Berger, J. Bonamy, and D. Robert, *Phys. Rev. A* **49**, 3396 (1994).
- <sup>20</sup> J. Brewer and G. W. Vaughn, *J. Chem. Phys.* **50**, 2960 (1969).
- <sup>21</sup> B. Schramm, E. Elias, and R. Pilger, *Chem. Phys. Lett.* **88**, 459 (1982).
- <sup>22</sup> J. A. Beswick and A. Requena, *J. Chem. Phys.* **72**, 3018 (1980).
- <sup>23</sup> S.-I. Chu and K. K. Datta, *J. Chem. Phys.* **76**, 5307 (1982).
- <sup>24</sup> R. J. Le Roy, G. C. Corey, and J. M. Hutson, *Faraday Discuss. Chem. Soc.* **73**, 339 (1982).
- <sup>25</sup> K. K. Datta and S.-I. Chu, *Chem. Phys. Lett.* **95**, 38 (1983).
- <sup>26</sup> J. M. Hutson and R. J. Le Roy, *J. Chem. Phys.* **78**, 4040 (1983).
- <sup>27</sup> I. F. Kidd and G. G. Balint-Kurti, *Chem. Phys. Lett.* **101**, 419 (1983).
- <sup>28</sup> I. F. Kidd and G. G. Balint-Kurti, *Chem. Phys. Lett.* **105**, 91 (1984).
- <sup>29</sup> I. F. Kidd and G. G. Balint-Kurti, *J. Chem. Phys.* **82**, 93 (1985).
- <sup>30</sup> I. F. Kidd and G. G. Balint-Kurti, *Faraday Discuss. Chem. Soc.* **82**, 241 (1986).
- <sup>31</sup> O. Roncero, S. Miret-Artés, G. Delgado-Barrio, and P. Villarreal, *J. Chem. Phys.* **85**, 2089 (1986).
- <sup>32</sup> G. Brocks, *Mol. Phys.* **62**, 1483 (1987).
- <sup>33</sup> J. A. Beswick and A. Requena, *J. Chem. Phys.* **73**, 4347 (1980).
- <sup>34</sup> J. M. Hutson, C. J. Ashton, and R. J. Le Roy, *J. Phys. Chem.* **87**, 2713 (1983).
- <sup>35</sup> R. J. Le Roy, in *Resonances in Electron-Molecule Scattering, van der Waals Complexes, and Reactive Chemical Dynamics*, ASC Symposium Series No. 263, edited by D. G. Truhlar (American Chemical Society, Washington, D. C., 1984), p. 231.
- <sup>36</sup> P. Villarreal, G. Delgado-Barrio, O. Roncero, E. de Pablo, and S. Miret-Artés, in *Structure and Dynamics of Weakly Bound Molecular Complexes*, NATO ASI Series, Series C, edited by A. Weber (Reidel, Dordrecht, 1987), Vol. 212, p. 583.
- <sup>37</sup> H. L. Williams, K. Szalewicz, B. Jeziorski, R. Moszynski, and S. Rybak, *J. Chem. Phys.* **98**, 1279 (1993).
- <sup>38</sup> D. W. Schwenke, S. P. Walch, and P. R. Taylor, *J. Chem. Phys.* **98**, 4738 (1993).
- <sup>39</sup> R. Moszynski, B. Jeziorski, P. E. S. Wormer, and A. van der Avoird, *Chem. Phys. Lett.* **221**, 161 (1994).
- <sup>40</sup> B. Jeziorski, R. Moszynski, and K. Szalewicz, *Chem. Rev.* **94**, 1887 (1994).
- <sup>41</sup> R. Moszynski, T. Korona, T. G. A. Heijmen, P. E. S. Wormer, A. van der Avoird, and B. Schramm, *Pol. J. Chem.* **72**, 1479 (1998).
- <sup>42</sup> H. Kreek and R. J. Le Roy, *J. Chem. Phys.* **63**, 338 (1975).
- <sup>43</sup> R. Moszynski, B. Jeziorski, A. van der Avoird, and P. E. S. Wormer, *J. Chem. Phys.* **101**, 2825 (1994).
- <sup>44</sup> T. Slee and R. J. Le Roy, *J. Chem. Phys.* **99**, 360 (1993).
- <sup>45</sup> A. C. Allison, *Adv. At. Mol. Phys.* **25**, 323 (1988).
- <sup>46</sup> F. Mrugała, *Int. Rev. Phys. Chem.* **12**, 1 (1993).
- <sup>47</sup> It should be noted, however, that because of the difficulties with measuring accurately the absorption of the complex when HD is in an excited state, cf. Ref. 6, the studies on the  $Q_1(1)$  (and also  $S_1(1)$ ) band(s) are less useful for the purpose of verification and/or improvement of intermolecular potentials.
- <sup>48</sup> G. G. Balint-Kurti and M. Shapiro, *Chem. Phys.* **61**, 137 (1981).
- <sup>49</sup> G. G. Balint-Kurti and M. Shapiro, *Adv. Chem. Phys.* **60**, 403 (1985).
- <sup>50</sup> G. Birnbaum, S.-I. Chu, A. Dalgarno, L. Frommhold, and E. L. Wright, *Phys. Rev. A* **29**, 595 (1984).
- <sup>51</sup> J. Schaefer and A. R. W. McKellar, *Z. Phys. D* **15**, 51 (1990).
- <sup>52</sup> L. Frommhold, *Collision-Induced Absorption in Gases* (Cambridge University Press, Cambridge, 1993).
- <sup>53</sup> F. T. Smith, *Phys. Rev.* **118**, 349 (1960).
- <sup>54</sup> R. G. Newton, *Scattering Theory of Waves and Particles* (Springer, New York, 1966).
- <sup>55</sup> Ch. J. Joachain, *Quantum Collision Theory* (North-Holland, Amsterdam, 1975).
- <sup>56</sup> R. D. Levine, *Quantum Mechanics of Molecular Rate Processes* (Clarendon, Oxford, 1969).
- <sup>57</sup> C. J. Ashton, M. S. Child, and J. M. Hutson, *J. Chem. Phys.* **78**, 4025 (1983).
- <sup>58</sup> S.-W. Cho, A. F. Wagner, B. Gazdy, and J. M. Bowman, *J. Chem. Phys.* **96**, 2812 (1992).
- <sup>59</sup> R. J. Le Roy and R. B. Bernstein, *J. Chem. Phys.* **54**, 5114 (1971).
- <sup>60</sup> F. Mrugała, *Mol. Phys.* **65**, 377 (1988).
- <sup>61</sup> Z. Drakjian, E. F. Hayes, G. A. Parker, E. A. Butcher, and J. D. Kress, *J. Chem. Phys.* **95**, 2516 (1991).
- <sup>62</sup> L. C. Biedenharn and J. D. Louck, *Angular Momentum in Quantum Physics* (Addison-Wesley, Reading, 1981).
- <sup>63</sup> W. J. Thompson, *Angular Momentum* (Wiley, New York, 1994).
- <sup>64</sup> Y. Sun, M. L. Du, and A. Dalgarno, *J. Chem. Phys.* **93**, 8840 (1990).
- <sup>65</sup> M. L. Du and A. Dalgarno, *Phys. Rev. A* **43**, 3474 (1991).
- <sup>66</sup> F. Mrugała, *J. Chem. Phys.* **91**, 874 (1989).
- <sup>67</sup> M. Shapiro, *J. Chem. Phys.* **56**, 2582 (1972).
- <sup>68</sup> M. Shapiro and G. G. Balint-Kurti, *J. Chem. Phys.* **71**, 1461 (1979).
- <sup>69</sup> J. M. Hutson, *Adv. Mol. Vib. Coll. Dyn.* **1A**, 1 (1991).
- <sup>70</sup> A. van der Avoird, P. E. S. Wormer, and R. Moszynski, *Chem. Rev.* **94**, 1931 (1994).
- <sup>71</sup> S. Bratoz and M. L. Martin, *J. Chem. Phys.* **42**, 1051 (1965).
- <sup>72</sup> W.-K. Liu, J. E. Grabenstetter, R. J. Le Roy, and F. R. McCourt, *J. Chem. Phys.* **68**, 5028 (1978).
- <sup>73</sup> J. M. Hutson, *Faraday Discuss. Chem. Soc.* **82**, 292 (1986).
- <sup>74</sup> L. Wolniewicz, *J. Chem. Phys.* **99**, 1851 (1993).
- <sup>75</sup> L. Wolniewicz, *J. Chem. Phys.* **103**, 1792 (1995).
- <sup>76</sup> F. Mrugała, *J. Chem. Phys.* **93**, 1257 (1990).
- <sup>77</sup> J. M. Brown, J. T. Hougen, K. P. Huber, J. W. C. Johns, I. Kopp, H. Lefebvre-Brion, A. R. Mere, D. A. Ramsay, J. Rostas, and R. N. Zare, *J. Mol. Spectrosc.* **55**, 500 (1975).